Selective inhibition mediates the sequential recruitment of motor pools

Maarten F. Zwart[1,2,*], Stefan R. Pulver[1,†], James W. Truman[1], Akira Fushiki[1], Albert Cardona[1,3,*], Matthias Landgraf[2,3]

[1]HHMI Janelia Research Campus, Ashburn, VA, 20147, USA

[2]Department of Zoology, University of Cambridge, Cambridge, CB2 3EJ, United Kingdom

[3]Co-senior author

[*]Correspondence: zwartm@janelia.hhmi.org or cardonaa@janelia.hhmi.org

[†]Current address: School of Psychology & Neuroscience, University of St Andrews, St Andrews, KY16 9JP, United Kingdom

Summary

Locomotor systems generate diverse motor patterns to produce the movements underlying behavior, requiring that motor neurons be recruited at various phases of the locomotor cycle. Reciprocal inhibition produces alternating motor patterns; however, the mechanisms that generate other phasic relationships between intrasegmental motor pools are unknown. Here, we investigate one such motor pattern in the *Drosophila* larva, using a multidisciplinary approach including electrophysiology and ssTEM-based circuit reconstruction. We find that two motor pools that are sequentially recruited during locomotion have identical excitable properties. In contrast, they receive input from divergent premotor circuits. We find that this motor pattern is not orchestrated by differential excitatory input, but by a GABAergic interneuron acting as a delay line to the later-recruited motor pool. Our findings show how a motor pattern is generated as a function of the modular organization of locomotor networks through segregation of inhibition, a potentially general mechanism for sequential motor patterns.

Introduction

Movements are generated by precise sequences of activity in motor systems. In spite of decades of research, the logic underlying the neural circuitry that produces these sequences during locomotion remains unclear (Büschges et al., 2011; Harris and Weinberg, 2012; McLean and Dougherty, 2015). Attempts to decipher this logic have largely focused on the alternating patterns of activity that underlie the recruitment of antagonistic motor units, such as flexors and extensors (Grillner, 2003; Grillner and Jessell, 2009; McLean and Dougherty, 2015; Talpalar et al., 2011; Tripodi et al., 2011), depressors and elevators (Burrows, 1996), and the bilaterally homologous motor units that underlie left-right alternation (Grillner, 2003; Talpalar et al., 2013). A common circuit motif that underlies these antiphasic activity patterns are reciprocal inhibitory connections between premotor circuits (Büschges et al., 2011; Kiehn, 2011).

However, many movements require gradual, overlapping sequences of muscle contractions. For instance, synergistic motor pools are tuned across the entire phasic space during fictive locomotion in the mouse spinal cord (Hinckley et al., 2015; Machado et al., 2015) and fictive scratching in the turtle (Berkowitz and Stein, 1994), and many intrasegmental muscles in the cat contract sequentially with overlaps in their activation during various movements (Pratt et al., 1991). In spite of the prominence of this type of motor pattern, it is unknown how premotor circuits generate the required sequential patterns of activity within each segment in the appropriate motor neurons.

In principle, the sequential pattern can be established through two, non-mutually exclusive mechanisms: first, a common source of interneuronal input could elicit temporally distinct responses in motor neurons that have different electrical properties

(Johnson et al., 2005; Matsushima et al., 1993; Wang and McLean, 2014). Second, premotor networks could recruit motor units sequentially through differences in the delivery of excitatory or inhibitory input (Bagnall and McLean, 2014; Gabriel et al., 2011). In locomotor networks, motor neurons are ordered centrally to represent the spatial organization of their postsynaptic muscles, forming a myotopic map that also extends to their presynaptic partners (Landgraf et al., 2003; Okado et al., 1990; Romanes, 1964; Sürmeli et al., 2011; Tripodi et al., 2011). This conserved feature mediates the segregation of input onto different classes of motor neurons and could form the basis for the generation of different motor patterns.

In this study we draw on the experimental advantages of the *Drosophila* larva to determine the neural basis for a motor pattern that is conceptually similar to the sequential pattern described in vertebrate motor systems. Specifically, we focus on delineating the circuit mechanisms underlying the generation of an intrasegmental sequence of overlapping contractions of two distinct muscle groups during larval crawling (Heckscher et al., 2012). First, using whole-cell electrophysiology, we show that motor neurons that innervate either muscle group do not differ in their intrinsic electrical properties, suggesting that their recruitment pattern must be the result of the organization of the presynaptic network. Second, reconstructions from ssTEM of the premotor network show that motor neurons that are recruited at different phases of the intrasegmental locomotor cycle receive input from largely different sets of interneurons. This contrasts with functionally similar motor neurons, which share a high degree of common input. Third, probing further into the premotor network, we find that the motor pattern is not orchestrated by differential excitatory inputs, but by a GABAergic inhibitory interneuron that specifically innervates the later-recruited class of motor neurons and acts as an intrasegmental delay line. Our results show that

79 the segregation of input onto distinct intrasegmental motor neurons facilitates the
80 generation of a widespread motor pattern through selective inhibition of a motor pool.
81 This might represent a general mechanism for generating non-alternating phase
82 relationships between intrasegmental motor pools.

83

Results

Motor neurons innervating functionally distinct muscles have similar intrinsic properties

Previous work established that locomotion in the *Drosophila* larva is mediated by peristaltic waves of muscle contractions, which, during forward locomotion, commence in posterior segments and propagate anteriorly from one segment to the next (Crisp et al., 2008). Within each segment, the longitudinal muscles, running parallel to the length of the animal, begin to contract before transverse muscles, which are oriented perpendicular to the main body axis (Heckscher et al., 2012; Fig. 1A, B). This is followed by a period of co-contraction of both muscle sets (Fig. 1A, B). Thus, this intrasegmental muscle contraction sequence is unlike alternating left-right or flexor-extensor activation, which have been a primary focus of studies in vertebrate model systems (Kiehn, 2011). This intrasegmental sequence is a signature of larval crawling in both first and third instar larvae (Heckscher et al., 2012; Pulver et al., 2015). The contractions represent highly coherent waveforms with contractions of transverse muscles occurring with a ~42˚ phase lag relative to longitudinal muscles during forward locomotion (Fig. 1C). Importantly, the sequence is generated independently of sensory feedback (Pulver et al., 2015), ruling out an essential role of the musculature or proprioception in setting this motor pattern. This motor pattern is therefore similar in concept to the sequential recruitment of synergistic intrasegmental motor pools in vertebrates.

We set out to study its neuronal basis. One underlying mechanism could be that the two sets of motor neurons that innervate longitudinal versus transverse muscles have different electrical properties, so that the same inputs would elicit temporally distinct

responses (Choi et al., 2004; Gabriel et al., 2011; Schaefer et al., 2010; Wang and McLean, 2014). In order to test whether the motor neurons innervating the transverse muscles have intrinsic properties that delay their firing relative to motor neurons innervating longitudinal muscles, we performed whole-cell recordings in current clamp and measured membrane voltages in response to steps and ramps of current injection in representative motor neurons (those innervating muscles Lateral Transverse 1-4 (MNs-LT1-4) and muscle Lateral Oblique 1 (MN-LO1), respectively (Fig. 1)). The membrane properties of these neurons were similar, with no statistical differences in membrane capacitance (C_m), input resistance (R_m), action potential threshold, or resting membrane potential (Fig. 1H-K, $p>0.05$). Indeed, the number of action potentials fired in response to different steps of current injection was the same for the two representative groups (Fig. 1L, $p>0.05$). Crucially, there is no difference in the onset of firing in response to depolarizing current injection, as quantified by the delay to first spike (Fig. 1I, $p>0.05$). During rhythmic activity of the *Drosophila* larval motor network, the firing properties of motor neurons can be modulated by the action of the Na^+/K^+-ATPase in response to bursts of action potentials (Pulver and Griffith, 2010). However, we found that with rhythmic current injections the delay to first spike does not deviate between the two groups of motor neurons (Fig. S1A, B, $p>0.05$). Furthermore, we could find no evidence of plateau potentials or rebound depolarizations in these cells (data not shown). Indeed, recording the action potentials these cells fire as the result of endogenous rhythmic excitatory input, we found no difference between the two groups of motor neurons in the duration between the onset of depolarization and the onset of firing (Fig. S1C, D, $p>0.05$). Taken together these electrophysiological data suggest that the intrasegmental motor pattern is not

mediated by differences in the intrinsic excitable properties of the output motor neurons. The data therefore point to divergence in premotor network input.

Functionally distinct motor neurons receive divergent input

Recent studies in vertebrate systems have suggested that functionally distinct motor units receive input from different complements of presynaptic neurons (Bagnall and McLean, 2014; Goetz et al., 2015; Stepien et al., 2010; Tripodi et al., 2011). Having established that the intrasegmental motor sequence in the *Drosophila* larva does not depend on the intrinsic properties of the output neurons, we next investigated the organization of the motor network presynaptic to representatives of the two different groups of motor neurons. To this end we took advantage of an ssTEM volume of an entire first instar larval CNS, which is currently being reconstructed in a community-based effort (Fushiki et al., 2016; Heckscher et al., 2015; Ohyama et al., 2015). Within this ssTEM volume we reconstructed in segment A1 MNs-LT1-4 as well as MN-LO1. These have the same axonal trajectory but distinct territories of dendritic arborization (Fig. 2A). Next, we reconstructed the morphologies of all presynaptic partners of these motor neurons, a total of 198 arbors from thoracic, abdominal and suboesophageal segments (Fig. S2; see Experimental Procedures for details). Out of 198 arbors, 111 different cell types could be identified based on morphology, providing 1300 (92%) of the total of 1409 input synapses onto the dendrites of both classes of motor neurons. Comparison of the complements of interneurons that are presynaptic to the two classes of motor neurons revealed a considerable degree of divergence between them (Fig. 2B-F). For example, MN-LT2 (representing a transverse muscle-motor neuron unit) and MN-LO1 (representing a longitudinal

muscle-motor neuron unit) receive 82% of their input synapses from different presynaptic partners. In contrast, operationally similar motor neurons receive the vast majority of their input from common partners (e.g., 82% between MN-LT1 and MN-LT2). In order to determine the significance of this divergence in presynaptic partners we compared the relative importance of the shared input between pairs of motor units: MN-LT1 and MN-LT2 versus MN-LT2 and MN-LO1. We find that presynaptic neurons that synapse onto two operationally similar motor neurons provide similar numbers of synapses to both (Fig. 2E; Pearson's $r=0.76$; $p<0.0001$). In contrast, where the same presynaptic neuron forms synaptic connections with two operationally distinct motor neurons, there is no such correlation (Fig. 2F; $p>0.05$). In other words, functionally distinct motor neurons share few presynaptic partners; moreover, those that are shared either make few synaptic connections to both, or are more strongly connected to only one of them, further emphasizing the significance of the divergence of the presynaptic network. This circuit architecture suggests that the characteristic intrasegmental motor sequence could indeed be the result of the organization of the premotor network.

The contribution of premotor excitatory drive to the motor pattern

The distinct premotor circuits of the two classes of motor neurons could reflect a functional segregation of excitatory input, capable of delivering temporally distinct excitation. To test this hypothesis, we probed the premotor network to find cell types that could provide this excitation.

First, we identified *GAL4* driver lines that allow visualization of discrete sets of pre-motor interneurons (Li et al., 2014), as identified by ssTEM reconstructions. Next, we

determined which of these interneuron types stained positive for the biosynthetic enzyme for the main excitatory neurotransmitter in this system, choline acetyltransferase (Baines et al., 1999). Among this subset we focused on those neurons that made more than 35 synaptic release sites onto the dendrites of the transverse muscle motor neurons MNs-LT1-4 (>2.75% of total number of synaptic sites), but not onto MN-LO1. We thus identified three contralaterally projecting interneuron types (Fig. 3, S3), excitatory Interneurons 1, 2, and 3 (eINs-1-3), derived from lineage 18/NB2-4 (eIN-1) and lineage 01/NB1-2 (eIN-2, eIN-3), respectively (Lacin and Truman, 2016). They are among the most strongly connected premotor interneurons within this premotor network, providing 14.6%, 13.5%, and 6.7% of total input synapses onto the transverse muscle motor neurons MNs-LT1-4 per segment, respectively. Moreover, each of these three excitatory interneurons also synapses onto other motor neurons innervating other transverse muscles, such as MN-DT1.

To assess whether eINs-1-3 could play a role in setting the intrasegmental phase relationship between MN-LO1 and the MNs-LT1-4 during larval crawling, we performed functional imaging of activity within these neurons. Specifically, we used a well characterized fictive crawling activity paradigm, in which the nerve cord has been isolated from the periphery (Berni, 2015; Pulver et al., 2015); Experimental Procedures). Because there is no clean GAL4 driver line for MN-LO1, we used the segmentally repeated aCC motor neuron as a robust indicator of fictive crawling phases and cycles (Fig. 3G, Fig. S3; (Pulver et al., 2015)). MN-aCC is readily identifiable using *RRF-GAL4* (Fujioka et al., 2003), while MN-LO1 and the transverse muscle motor neurons MNs-LT1-4 selectively express Gal4 in the *B-H1-GAL4* line (Garces et al., 2006; Sato et al., 1999). Using these reagents and paired

whole-cell recording of their activity during fictive crawling we established that, consistent with their both innervating longitudinal muscles, the MN-aCC and MN-LO1 motor neurons are active in phase during fictive locomotion (Fig. S4).

We then measured fluorescence changes of the genetically encoded calcium indicator GCaMP6f (Chen et al., 2013) selectively expressed in a given eIN (see Experimental Procedures for details on driver lines) and the phase reference marker, MN-aCC. This experiment therefore allowed us to determine whether eIN-1, eIN-2, and eIN-3 are recruited during locomotion and to relate their activity to the activity pattern of the early recruited MN-aCC (active in the same phase as MN-LO1).

We found that all three eINs show wave-like activity during fictive locomotion (Fig. 3G, H, Fig. S3), with GCaMP6f dynamics highly coherent with those of the MN-aCC. Unexpectedly, the eIN activity dynamics are closest in phase with the MN-aCC located within the same segment, which is an early-recruited, longitudinal muscle motor neuron (Fig. 3I, Fig. S3). Therefore these results do not support the hypothesis of sequential excitation generating the sequential intrasegmental motor pattern.

In order to further probe the role of excitation in the intrasegmental motor pattern, we decided to investigate the excitatory drive to the early recruited MN-LO1. This motor neuron receives input from many different cell types (a total of 70 arbors, providing a mean of 2.4 synapses each). We focused our efforts on the three most strongly connected cell types, which we named eINs-4-6. Collectively, eIN-4-6 provide 49 synapses (28.9% of MN-LO1 input) and, staining positive for choline acetyltransferase (Fig. S4), are presumed excitatory. We characterized the activity patterns of these neurons during fictive locomotion. As before, we related the activity of eINs-4-6 to the activity of the segmentally repeated MN-aCC motor neuron by

selectively expressing GCaMP6f both in a given eIN and in the phase reference marker MN-aCC (see Experimental Procedures for details on driver lines). We found that eINs-4-6 all show wave-like activity during fictive locomotion (Fig. S4), and, similar to eIN-1-3, are highly coherent and closest in phase with the MN-aCC in the segment they innervate (Fig. S5). These results indicate that the main excitatory premotor interneurons of both early recruited MN-LO1 and those of the later recruited MNs-LTs have temporally similar recruitment patterns, in phase with MN-aCC. This strongly suggests that temporally distinct excitatory drive is unlikely to underlie the sequential motor pattern.

In order to further probe the role of the eINs in the generation of the motor pattern, we performed optogenetic stimulation of eINs-1-3, which are presynaptic to the MNs-LTs. We selectively expressed *UAS-CsChrimson* (Klapoetke et al., 2014) in eIN1-3, one cell type at a time, and assessed the effect of stimulating these neurons by measuring contractions of the transverse muscle LT2 and longitudinal muscle LO1 in a novel semi-intact preparation that exhibits the characteristic intrasegmental motor sequence (see Experimental Procedures). Acute, high level stimulation (617 nm, 1.1 mW/mm^2) of eIN1, eIN2 or eIN3 induces contraction of muscle LT2, but not muscle LO1 (Fig. 3J, Fig. S3), suggesting that these neurons are indeed capable of driving the MNs-LT selectively and efficiently. Interestingly, chronic, low level stimulation (617 nm, $0.01mW/mm^2$) of any of these eINs caused muscle LT2 to contract earlier than normal in the locomotor cycle, thus reducing the phase offset between LT2 and LO1 contractions (Fig. 3K, L, Fig. S3) ($p<0.05$, Hotelling paired test, $n\geq5$). This excitation level-dependent shift in the recruitment of MNs-LTs suggests that during the normal locomotion cycle the delay MNs-LTs recruitment cycle might be effected by a source of inhibition on to the MNs-LTs.

The intrasegmental motor sequence depends on GABAergic or glutamatergic inhibition

In various other motor systems (Grillner and Jessell, 2009; Kiehn, 2011) inhibitory inputs generate alternating sequences of muscle activation. We reasoned that the observed segregation of input in our system may reflect differences in inhibition that underlie the pattern of activation of the two classes of motor neurons examined. We therefore performed muscle-imaging experiments in our semi-intact preparation (see Experimental Procedures). We then bath-applied picrotoxin (PTX, 10^{-6}M) to block glutamate and GABA-gated Cl^--channel-mediated inhibition (Liu and Wilson, 2013; Mauss et al., 2014; Rohrbough and Broadie, 2002). Whereas in control experiments the longitudinal and transverse muscle groups contract in sequence, we found that application of PTX effectively and selectively changes this motor pattern: while intersegmental waves remain intact, the longitudinal and transverse muscle groups within each segment now contract in synchrony (Fig. 3D-F; Hotelling paired test, $p<0.01$, $n=5$). This suggests that the motor network provides a source of picrotoxin-sensitive inhibition that mediates the motor sequence.

A GABAergic cell type presynaptic to one class of motor neurons is required for the motor pattern

We reasoned that the source of the inhibition that generates the intrasegmental motor sequence likely resides within the network that is presynaptic to the later firing, transverse muscle motor neurons. To test this hypothesis, we identified within the

277 extensive premotor network cells that: i) contain GABA neurotransmitter; ii)
278 exclusively innervate the transverse muscle motor neurons; iii) are recruited during
279 locomotion; iv) are functionally required for the intrasegmental motor sequence.

280 First, we determined which of the premotor cell types found in our ssTEM
281 reconstructions stained positive for the neurotransmitter GABA, and then selected
282 those that made more than 35 synaptic release sites exclusively onto the dendrites of
283 the transverse motor neurons (>2.75% of total number of synaptic sites; same
284 threshold as for eINs). We thus identified three contralaterally projecting interneuron
285 types (Fig. 5; data not shown for iIN-2 and -3), inhibitory Interneurons 1, 2 and 3
286 (iIN-1-3), which provide 2.8%, 15.1%, and 9.8% of total input synapses onto the
287 transverse muscle motor neurons per segment, respectively. Moreover, the majority of
288 postsynaptic neurons of iINs-1-3 that could be identified are motor neurons with
289 target muscles of similar orientation as muscles LT1-4 (Fig. 5F). These three
290 interneuron cell types therefore meet the first two selection criteria.

291 Next, to determine which of these iINs are recruited during locomotion, we performed
292 functional imaging of neuronal activity as before. We found that only iIN-1, derived
293 from abdominal lineage 14/NB4-1 (Lacin and Truman, 2016), shows wave-like
294 activity during fictive locomotion (Fig. 5G, H; data not shown for iIN-2 and -3). iIN-1
295 GCaMP6f activity is highly coherent with that of MN-aCC, and is closest in phase to
296 the aCC motor neuron located within the same segment (Fig. 5I). Therefore, only iIN-
297 1 fulfills all 3 criteria: it has a transmitter complement and activity profile consistent
298 with it having the potential for introducing a delay in firing between longitudinal and
299 transverse muscle motor neurons.

To determine whether the activity of iIN-1 is required to generate the sequential intrasegmental motor pattern, we performed muscle-imaging experiments in animals in which we selectively inhibited the output of iIN-1 by expressing the hyperpolarizing potassium channel Kir2.1 (Baines et al., 2001). We found that targeting the expression of *UAS-Kir2.1* to iIN-1 using *R83H09-GAL4* interferes with the motor pattern: with each peristaltic wave, the intrasegmental sequence of muscle contractions that is normally observed is changed, so that now both muscle groups contract largely in synchrony (Fig. 6A-C; also see Fig. S6. p=0.003, n=7). These results are consistent with our observation that the excitatory drive to the transverse muscle motor neurons is in phase with activation of the longitudinal motor pool. We noticed that, while *R83H09-GAL4* expresses in iIN-1 in all abdominal segments, it also expresses in other, as yet unidentified, cell types in abdominal, thoracic and suboesophageal segments and the brain (Fig. 6D). We therefore repeated the experiment using a more selective intersectional "Split-GAL4" driver line, *SS01411-GAL4*, which expresses exclusively in iIN-1, though in a smaller number of abdominal segments (Fig. 6D). The intrasegmental motor pattern defects seen with *SS01411-GAL4* targeted expression of *UAS-Kir2.1* were indistinguishable from those seen with *R83H09-GAL4* (Fig. 6C, p=0.004, n=5). To further test the outcome of the experiments we interfered with iIN-1 synaptic transmission in a different way, by targeting expression of *UAS-TeTxLC*, which prevents evoked neurotransmitter release (Sweeney et al., 1995), This has the same disruptive effect on the intrasegmental motor pattern as expressing Kir2.1 (Fig. 6C, p=0.0005, n=6).

The data suggest that the activity of iIN-1 might act as a delay line to the transverse muscle motor neurons and that this determines the intrasegmental motor pattern. If this is indeed the case, then, we reasoned, experimentally elevated levels of activity of

iIN-1 should cause an enhanced phase shift between muscle contractions of LT2 versus LO1 during fictive crawling. To test this hypothesis, we optogenetically activated iIN-1 using *UAS-CsChrimson* expressed in iIN-1 with *R83H09-GAL4* and assessed the effect on the motor pattern during fictive crawling in our semi-intact preparation. Acute, high-level stimulation of this iIN-1 (617 nm, 1.1 mW/mm^2) led to relaxation of muscle LT2 whilst leaving muscle LO1 unaffected (Fig. 6E). Consistent with our hypothesis that iIN-1 acts as a delay line to the transverse muscle motor neurons, low-level stimulation of iIN-1 (617 nm, 0.1 mW/mm^2) caused an increase in the phase shift between muscles LO1 and LT2 (Hotelling paired test, $p<0.05$, $n=7$). Taken together, our results suggest that the intrasegmental phase relationship between the longitudinal and transverse motor units is set by the subset-specific inhibitory interneuron iIN-1. Moreover, iIN-1 seems to act as a delay line that modulates the effects of otherwise co-incident excitation to both motor pools.

Discussion

The circuit mechanisms that generate movements have been studied for many decades, in large part focused on the alternating contractions of antagonistic muscles such as flexors and extensors (Büschges et al., 2011; Goulding, 2009; Kiehn, 2011; Miri et al., 2013). However, many motor pools are recruited sequentially, in largely overlapping patterns of activity (Berkowitz and Stein, 1994; Hinckley et al., 2015; Machado et al., 2015; Pratt et al., 1991). In this study we investigate the neural mechanisms of such a pattern, focusing on an intrasegmental sequence of muscle contractions that is characteristic for larval crawling. Working with the *Drosophila*

larva we demonstrate that motor neurons that are recruited at different phases of the intrasegmental locomotor cycle receive largely divergent input and that the activity of an identified inhibitory interneuron is required for generating the phase delay.

Intrinsic excitable properties and the recruitment of motor neurons

The output of a neural network is shaped by the intrinsic properties of its constituent neurons. For instance, the biophysical properties of different motor neuron populations in part determine their differential recruitment in the zebrafish spinal cord (Gabriel et al., 2011; McLean et al., 2007). In the *Drosophila* larva, a delay to action potential firing is mediated by a *Shal*-encoded I_A-current in the RP2 motor neuron (Choi et al., 2004; Schaefer et al., 2010). Focusing on the motor neurons that are sequentially recruited during larval crawling, we found no evidence of differences in their electrical properties. Instead we found that the sequential intrasegmental recruitment is due to differences in the synaptic input that these different motor units receive.

Segregation of premotor connectivity

For many sensory systems, axon terminals are arranged in the central nervous system (CNS) to form neural representations of sensory neuron modality and topography (Fitzpatrick and Ulanovsky, 2014). This straightforward link between neuronal anatomy and function has been less clear in motor systems. In the mouse spinal cord, the dorsal-ventral segregation of motor pools pre-figures sensory-motor connectivity (Sürmeli et al., 2011), and largely spatially segregated sets of interneurons connect to

antagonistic motor neurons that innervate flexor and extensor muscles in the mouse (Tripodi et al., 2011).

Here, we characterized with single-synapse resolution the premotor circuitry of operationally different motor neurons in the *Drosophila* larva by EM-based reconstructions. This allowed us to establish that the myotopic organization of motor neurons is accompanied by a similarly segregated divergence of their presynaptic inputs: functionally similar motor neurons share many of their presynaptic partners (34/75 (45%) for MN-LT1 and MN-LT2), whereas functionally distinct motor neurons share few (9/112 (8%) between MN-LT2 and MN-LO1). Moreover, functionally similar motor neurons receive the majority of their synaptic input from shared presynaptic partners (82% of synapses provided by 45% of all presynaptic cells). In contrast, operationally distinct motor neurons share few presynaptic partners, and these are generally more strongly to only one of the motor neurons or weakly connected to both.

As a note of caution, in our EM analysis, given previous evidence, we assumed that synapse number positively correlates with synapse strength. First, the number of synapses between two cells in this system was found to positively correlate with the responsiveness of the postsynaptic cell to presynaptic stimulation (Ohyama et al., 2015). Second, at the larval neuromuscular junction the strength of the postsynaptic response also correlates with synapse number (Budnik and Ruiz-Canada, 2006; Büschges et al., 2011; McLean and Dougherty, 2015). Third, we found little variability in the size of pre- and postsynaptic densities within the CNS of the *Drosophila* larva (M. Zwart and A. Cardona, unpublished observation), in marked contrast to synapses in mammals, which can range in size over several orders of magnitude (Harris and Weinberg, 2012; Talpalar et al., 2011; Tripodi et al., 2011).

These strands of evidence suggest that the number of synapses between central neurons likely correlates with the physiological relevance of connections.

Divergent input and the generation of different motor patterns

It has been proposed that alternating muscle contractions are generated by largely divergent sets of premotor neurons, providing the antiphasic rhythmic drive through reciprocal inhibitory interactions (Grillner, 2003; Kiehn, 2011; Talpalar et al., 2011). It has been unclear how more gradual, overlapping sequences of muscle contractions, which are common to most movements, are generated (Bellardita and Kiehn, 2015; Berkowitz and Stein, 1994; Hinckley et al., 2015; Machado et al., 2015; Pratt et al., 1991). In the zebrafish, different groups of motor neurons are incrementally recruited with increasing swimming speeds by distinct sub-populations of V2a excitatory interneurons (Ampatzis et al., 2014; Gabriel et al., 2011; McLean et al., 2008). In the larval *Drosophila* motor network we found that sequentially recruited groups of motor neurons receive input from different complements of interneurons. Unexpectedly, we found that the sets of excitatory pre-motor interneurons that innervate the early and late acting motor pools are recruited in phase. Instead, we found that the sequential motor pool recruitment is generated by the GABAergic premotor interneuron iIN-1, which selectively innervates the later recruited MNs-LTs. Furthermore, chronic, low-level optogenetic stimulation of this inhibitory neuron caused the MNs-LTs to be recruited later in the locomotor cycle, while low-level stimulation of the eINs presynaptic to MNs-LT caused their earlier recruitment. Our data are compatible with a model in which the balance between excitation and inhibition shapes the phase delay, with the iIN-1 in effect acting as a delay line for the later recruited transverse

muscle motor neurons. An obvious functional implication of the segregated and diversified architecture is an inherent capacity for generating distinct motor patterns by differentially recruiting premotor elements, thereby mediating the ability to perform the diverse movements underlying the animal's behavioral repertoire. For example, one could envisage how selective recruitment of iIN-1 could mediate a switch from a behavior in which the longitudinal and transverse muscles contract in sequence (e.g. crawling) to another in which they co-contract. In this light, it will be interesting to see whether similar segregated sources of inhibition mediate the generation of gradual sequences of muscle contractions in other systems, such as those innervating synergistic muscles in vertebrates (Bikoff et al., 2016; Goetz et al., 2015; Laine et al., 2015; Tripodi et al., 2011).

Conclusions

We have identified a circuit motif embedded in the myotopic map that generates the sequential contraction of two muscle groups, which is characteristic for crawling in *Drosophila* larvae. Our findings on the segregated premotor circuitry are consistent with reports from mouse and zebrafish (Bagnall and McLean, 2014; Tripodi et al., 2011) suggesting that their last common ancestor contained a modular motor system that evolved to support the axial and limb networks that allow for the differential control of muscles (Büschges et al., 2011). Similar circuit motifs may be responsible for sequential motor patterns manifest in many behavior across the animal kingdom.

Experimental procedures

Animal rearing and fly strains

All animals were raised at 25°C on standard corn meal based food, supplemented with all-trans retinal (1 mM) in the case of optogenetic stimulation experiments. 1st instar larvae were used in the ssTEM data; feeding 3rd instar larvae were used for all other experiments. We used the following genotypes: *w-;+;B-H1-GAL4* (Sato et al., 1999) crossed to *UAS-mCD8::GFP* animals for electrophysiology; *w-;UAS-GCaMP6f; RRF-GAL4* (Chen et al., 2013; Fujioka et al., 2003) crossed to *w-;R83H09-GAL4* or *w-;R09A07-GAL4* from the Rubin collection, or the split-GAL4 drivers (Luan et al., 2006; Pfeiffer et al., 2010) *SS01956-GAL4*, *SS01404-GAL4*, *SS01379-GAL4*, *SS02056-GAL4*, *SS01411-GAL4*, and *SS01970-GAL4*, based on the Rubin collection for GCaMP6f imaging; the muscle marker line *w-;G203;ZCL2144* (Crisp et al., 2008) for Figure 4; *w-;UAS-Kir2.1* (Baines et al., 2001) and *w-;UAS-TeTxLC* (Sweeney et al., 1995) to inhibit neural activity; *w-;UAS-CsChrimson::mVenus* (Klapoetke et al., 2014) crossed to the appropriate *GAL4* driver lines for optogenetic stimulation. The 'FLP-out' approach for stochastic single-cell labeling (MCFO) was described in detail elsewhere (Nern et al., 2015).

Reconstruction of premotor circuits using ssTEM data

ssTEM data were analyzed as described in Ohyama *et al.*, 2015. Motor neurons were identified and reconstructed within the ssTEM volume based on their axonal projection patterns (all MNs-LT and MN-LO1 assessed here project through nerve SNa (Landgraf et al., 1997)), cell body position, and dendritic morphologies (Lupton et al., *in preparation*). All synapses onto these motor neurons were annotated and used to identify and reconstruct all presynaptic partners.

Electrophysiology

All electrophysiology experiments were performed as described in Marley and Baines (2011). The fluorescent dye Alexa Fluor 568 Hydrazide (100 μM, ThermoFisher Scientific) was added to the intracellular solution to aid identification of patched neurons. Data were collected with a Multi-clamp 700B amplifier and digitized at 10kHz using a Digidata 1550 (both Molecular Devices, Sunnyvale, CA). Recordings were analyzed using custom scripts in Spike2 (Cambridge Electronic Design, Cambridge, UK).

Immunohistochemistry

Immunohistochemistry was performed as described in (Li et al., 2014). We dissected out larval CNSs as described before (Zwart et al., 2013), and fixed them in 4% paraformaldehyde for 30 minutes at room temperature to stain for GABAergic interneurons, or in Bouin's fixative for 5 minutes at room temperature to stain for cholinergic interneurons. Antibodies used were polyclonal anti-GABA antibody (Sigma-Aldrich, St Louis, MO; 1:200), or monoclonal ChAT-4B1 antibody (DSHB Hybridoma Product ChAT4B1, deposited to the DSHB by Salvaterra, P.M.; 1:100). Images were taken with a 710 laser-scanning confocal microscope (Zeiss) using a 20X/0.8 NA objective and contrast-adjusted using Fiji software (Schindelin et al., 2012).

Calcium imaging

For all calcium imaging experiments, we used a 488nm diode laser (Thorlabs) in conjunction with a spinning disk confocal imager (Crest X-Light) mounted on an Olympus BX51WI microscope. We collected images at 5-10 Hz with an Andor iXon Ultra 897 EMCCD camera (Andor Technologies, Belfast, UK) using Winfluor

software (John Dempster, University of Strathclyde), which was also used to drive the piezo-controller (Physik Instrumente, Karlsruhe, Germany) moving the objective (Olympus, 20X/1.0 NA) for generating z-stacks. Custom Matlab scripts were used to measure and extract changes in fluorescence in regions of interest. Optical signals were then visualized and analyzed in Fiji, Matlab, and Spike2.

Live imaging of muscle activity

We developed a semi-intact preparation to record contractions of muscles with reduced sensory feedback. 3rd instar larvae were dissected as in (Pulver and Griffith, 2010), but 2-3 segmental nerve roots were left intact. We loosely pinned the preparation to a Sylgard®-covered dish. Individual muscle contractions within innervated segments were then imaged using a 10X objective on an Olympus BX51WI microscope. The aperture of the field diaphragm was reduced to ensure the nervous system was not illuminated. The posterior and anterior attachment points of the Lateral Oblique muscle 1 (LO1, also known as m5) as well as the medial and lateral attachment points of Lateral Transverse muscle 2 (LT2, also known as m22) were tracked using the Manual Tracking plugin (Fiji). Muscle length was calculated and used as a measure of muscle activation. In a subset of experiments, we applied 10^{-6} M picrotoxin (Sigma-Aldrich, St Louis, MO) to preparations by manually exchanging the bath solution with a Pasteur pipette. For optogenetic stimulation experiments, 617 nm light provided by an OptoLED light source (Cairn, Faversham, UK) was delivered onto the preparation through the objective.

Coherence analysis of periodic activity

To determine the phase relationship between periodic signals in calcium imaging and muscle imaging experiments we used direct multi-taper estimates of power spectra and coherency (Cacciatore et al., 1999; Percival and Walden, 1993; Pulver et al., 2015; Taylor et al., 2003). In all experiments, we first performed a Fast Fourier Transform of the reference waveform (either the LO1 muscle or MN-aCC) in order to determine its spectral composition. We then determined the frequency at which the reference signal had the greatest power (the "dominant" frequency) and compared the coherence and phase relationship at that particular frequency between the reference signal and the other muscles or neurons, as appropriate. This analysis can efficiently compare the phase relationships between relatively complex waveforms, while attaching less weight to the peaks of activity, which are generally less informative in this context. Estimates were calculated with a time-bandwidth product of 5 and 7 tapers. All spectral calculations were carried out using custom scripts written in Matlab, now freely available online (https://github.com/JaneliaSciComp/Groundswell).

Statistics

Throughout the text, values are given in mean ± standard error unless otherwise stated. We tested data for normality using the Shapiro-Wilk test, with a=0.05. When data were normally distributed, *t* tests were used to test for significant differences. Otherwise, two-sample Wilcoxon tests were used. Linear regression, non-linear fitting of curves, and correlation analyses were performed in Prism (GraphPad Software), angular statistical analyses of results obtained with coherency analysis were carried out in Oriana. $p<0.05$ was considered statistically significant in all experiments.

Author contributions:

MFZ devised the project, co-wrote the manuscript, performed all experiments and analyses, and most EM reconstructions. SRP co-wrote the manuscript, developed the semi-intact preparation and contributed to the muscle imaging experiments. JWT characterized expression of GAL4-driver lines and is responsible for the identification of most larval cell types. AF contributed to reconstructions. AC and ML co-wrote the manuscript and supervised the project.

Acknowledgements:

We would like to thank Casey Schneider-Mizell for help training MFZ in EM reconstruction, generating Fig. 2C, and contributing to EM reconstructions, Karen Hibbard and other members of the fly facility, Adam Taylor from Janelia Scientific Computing and William Rowell from Janelia Technical resources for technical assistance, and Aref Arzan Zarin, Ingrid Andrade, and Philipp Schlegel for their contributions to EM reconstructions. We would also like to thank Gerry Rubin and Marta Zlatic for contributing GAL4 lines and Misha Ahrens, Vivek Jayaraman, Gareth Miles and Ellie Heckscher for valuable comments on the manuscript. This work was supported by the Howard Hughes Medical Institute, the HHMI Janelia Visitor Program (MFZ and ML), an Isaac Newton Trust/ISSF Wellcome Trust and a Wellcome Trust grant (092986/Z) to ML.

References

Ampatzis, K., Song, J., Ausborn, J., Manira, El, A., 2014. Separate microcircuit modules of distinct v2a interneurons and motoneurons control the speed of locomotion. Neuron 83, 934–943. doi:10.1016/j.neuron.2014.07.018

Ausborn, J., Stein, W., Wolf, H., 2007. Frequency control of motor patterning by negative sensory feedback. J Neurosci 27, 9319–9328. doi:10.1523/JNEUROSCI.0907-07.2007

Bagnall, M.W., McLean, D.L., 2014. Modular organization of axial microcircuits in zebrafish. Science 343, 197–200. doi:10.1126/science.1245629

Baines, R.A., Robinson, S.G., Fujioka, M., Jaynes, J.B., Bate, M., 1999. Postsynaptic expression of tetanus toxin light chain blocks synaptogenesis in Drosophila. Curr Biol 9, 1267–1270.

Baines, R.A., Uhler, J.P., Thompson, A., Sweeney, S.T., Bate, M., 2001. Altered electrical properties in Drosophila neurons developing without synaptic transmission. J Neurosci 21, 1523–1531.

Bellardita, C., Kiehn, O., 2015. Phenotypic characterization of speed-associated gait changes in mice reveals modular organization of locomotor networks. Curr Biol 25, 1426–1436. doi:10.1016/j.cub.2015.04.005

Berkowitz, A., Stein, P.S., 1994. Activity of descending propriospinal axons in the turtle hindlimb enlargement during two forms of fictive scratching: broad tuning to regions of the body surface. The Journal of Neuroscience 14, 5089–5104.

Berni, J., 2015. Genetic dissection of a regionally differentiated network for exploratory behavior in Drosophila larvae. Curr Biol 25, 1319–1326. doi:10.1016/j.cub.2015.03.023

Bikoff, J.B., Gabitto, M.I., Rivard, A.F., Drobac, E., Machado, T.A., Miri, A., Brenner-Morton, S., Famojure, E., Diaz, C., Alvarez, F.J., Mentis, G.Z., Jessell, T.M., 2016. Spinal Inhibitory Interneuron Diversity Delineates Variant Motor Microcircuits. Cell 165, 207–219. doi:10.1016/j.cell.2016.01.027

Budnik, V., Ruiz-Canada, C., 2006. The fly neuromuscular junction: structure and function. Elsevier.

Burrows, M., 1996. The neurobiology of an insect brain. Oxford University Press.

Büschges, A., Scholz, H., Manira, El, A., 2011. New moves in motor control. Curr Biol 21, R513–24. doi:10.1016/j.cub.2011.05.029

Cacciatore, T.W., Brodfuehrer, P.D., Gonzalez, J.E., Jiang, T., Adams, S.R., Tsien, R.Y., Kristan, W.B., Kleinfeld, D., 1999. Identification of neural circuits by imaging coherent electrical activity with FRET-based dyes. Neuron 23, 449–459.

Chen, T.-W., Wardill, T.J., Sun, Y., Pulver, S.R., Renninger, S.L., Baohan, A., Schreiter, E.R., Kerr, R.A., Orger, M.B., Jayaraman, V., Looger, L.L., Svoboda, K., Kim, D.S., 2013. Ultrasensitive fluorescent proteins for imaging neuronal activity. Nature 499, 295–300. doi:10.1038/nature12354

Choi, J.C., Park, D., Griffith, L.C., 2004. Electrophysiological and morphological characterization of identified motor neurons in the Drosophila third instar larva central nervous system. Journal of Neurophysiology 91, 2353–2365. doi:10.1152/jn.01115.2003

Crisp, S., Evers, J.F., Fiala, A., Bate, M., 2008. The development of motor coordination in Drosophila embryos. Development 135, 3707–3717. doi:10.1242/dev.026773

Fitzpatrick, D., Ulanovsky, N., 2014. Neural maps. Curr Opin Neurobiol 24, iv–vi. doi:10.1016/j.conb.2013.12.008

615 Fujioka, M., Lear, B.C., Landgraf, M., Yusibova, G.L., Zhou, J., Riley, K.M., Patel,
616 N.H., Jaynes, J.B., 2003. Even-skipped, acting as a repressor, regulates axonal
617 projections in Drosophila. Development 130, 5385–5400. doi:10.1242/dev.00770
618 Fushiki, A., Zwart, M.F., Kohsaka, H., Fetter, R.D., Cardona, A., Nose, A., 2016. A
619 circuit mechanism for the propagation of waves of muscle contraction in
620 Drosophila. Elife 5. doi:10.7554/eLife.13253
621 Gabriel, J.P., Ausborn, J., Ampatzis, K., Mahmood, R., Eklöf-Ljunggren, E., Manira,
622 El, A., 2011. Principles governing recruitment of motoneurons during swimming
623 in zebrafish. Nat Neurosci 14, 93–99. doi:10.1038/nn.2704
624 Garces, A., Bogdanik, L., Thor, S., Carroll, P., 2006. Expression of Drosophila
625 BarH1-H2 homeoproteins in developing dopaminergic cells and segmental nerve
626 a (SNa) motoneurons. Eur J Neurosci 24, 37–44. doi:10.1111/j.1460-
627 9568.2006.04887.x
628 Goetz, C., Pivetta, C., Arber, S., 2015. Distinct limb and trunk premotor circuits
629 establish laterality in the spinal cord. Neuron 85, 131–144.
630 doi:10.1016/j.neuron.2014.11.024
631 Goulding, M., 2009. Circuits controlling vertebrate locomotion: moving in a new
632 direction. Nat Rev Neurosci 10, 507–518. doi:10.1038/nrn2608
633 Grillner, S., 2003. The motor infrastructure: from ion channels to neuronal networks.
634 Nat Rev Neurosci 4, 573–586. doi:10.1038/nrn1137
635 Grillner, S., Jessell, T.M., 2009. Measured motion: searching for simplicity in spinal
636 locomotor networks. Curr Opin Neurobiol 19, 572–586.
637 doi:10.1016/j.conb.2009.10.011
638 Harris, K.M., Weinberg, R.J., 2012. Ultrastructure of synapses in the mammalian
639 brain. Cold Spring Harbor Perspectives in Biology 4.
640 doi:10.1101/cshperspect.a005587
641 Heckscher, E.S., Lockery, S.R., Doe, C.Q., 2012. Characterization of Drosophila
642 larval crawling at the level of organism, segment, and somatic body wall
643 musculature. J Neurosci 32, 12460–12471. doi:10.1523/JNEUROSCI.0222-
644 12.2012
645 Heckscher, E.S., Zarin, A.A., Faumont, S., Clark, M.Q., Manning, L., Fushiki, A.,
646 Schneider-Mizell, C.M., Fetter, R.D., Truman, J.W., Zwart, M.F., Landgraf, M.,
647 Cardona, A., Lockery, S.R., Doe, C.Q., 2015. Even-Skipped(+) Interneurons Are
648 Core Components of a Sensorimotor Circuit that Maintains Left-Right Symmetric
649 Muscle Contraction Amplitude. Neuron 88, 314–329.
650 doi:10.1016/j.neuron.2015.09.009
651 Hinckley, C.A., Alaynick, W.A., Gallarda, B.W., Hayashi, M., Hilde, K.L., Driscoll,
652 S.P., Dekker, J.D., Tucker, H.O., Sharpee, T.O., Pfaff, S.L., 2015. Spinal
653 Locomotor Circuits Develop Using Hierarchical Rules Based on Motorneuron
654 Position and Identity. Neuron 87, 1008–1021. doi:10.1016/j.neuron.2015.08.005
655 Johnson, B.R., Schneider, L.R., Nadim, F., Harris-Warrick, R.M., 2005. Dopamine
656 modulation of phasing of activity in a rhythmic motor network: contribution of
657 synaptic and intrinsic modulatory actions. Journal of Neurophysiology 94, 3101–
658 3111. doi:10.1152/jn.00440.2005
659 Kiehn, O., 2011. Development and functional organization of spinal locomotor
660 circuits. Curr Opin Neurobiol 21, 100–109. doi:10.1016/j.conb.2010.09.004
661 Klapoetke, N.C., Murata, Y., Kim, S.S., Pulver, S.R., Birdsey-Benson, A., Cho, Y.K.,
662 Morimoto, T.K., Chuong, A.S., Carpenter, E.J., Tian, Z., Wang, J., Xie, Y., Yan,
663 Z., Zhang, Y., Chow, B.Y., Surek, B., Melkonian, M., Jayaraman, V.,
664 Constantine-Paton, M., Wong, G.K.-S., Boyden, E.S., 2014. Independent optical

excitation of distinct neural populations. Nat. Methods 11, 338–346. doi:10.1038/nmeth.2836
Lacin, H., Truman, J.W., 2016. Lineage mapping identifies molecular and architectural similarities between the larval and adult Drosophila central nervous system. Elife 5. doi:10.7554/eLife.13399
Laine, C.M., Martinez-Valdes, E., Falla, D., Mayer, F., Farina, D., 2015. Motor Neuron Pools of Synergistic Thigh Muscles Share Most of Their Synaptic Input. J Neurosci 35, 12207–12216. doi:10.1523/JNEUROSCI.0240-15.2015
Landgraf, M., Bossing, T., Technau, G.M., Bate, M., 1997. The origin, location, and projections of the embryonic abdominal motorneurons of Drosophila. J Neurosci 17, 9642–9655.
Landgraf, M., Jeffrey, V., Fujioka, M., Jaynes, J.B., Bate, M., 2003. Embryonic origins of a motor system: motor dendrites form a myotopic map in Drosophila. PLoS Biol 1, E41. doi:10.1371/journal.pbio.0000041
Li, H.-H., Kroll, J.R., Lennox, S.M., Ogundeyi, O., Jeter, J., Depasquale, G., Truman, J.W., 2014. A GAL4 driver resource for developmental and behavioral studies on the larval CNS of Drosophila. CellReports 8, 897–908. doi:10.1016/j.celrep.2014.06.065
Liu, W.W., Wilson, R.I., 2013. Glutamate is an inhibitory neurotransmitter in the Drosophila olfactory system. Proceedings of the National Academy of Sciences 110, 10294–10299. doi:10.1073/pnas.1220560110
Luan, H., Peabody, N.C., Vinson, C.R., White, B.H., 2006. Refined spatial manipulation of neuronal function by combinatorial restriction of transgene expression. Neuron 52, 425–436. doi:10.1016/j.neuron.2006.08.028
Machado, T.A., Pnevmatikakis, E., Paninski, L., Jessell, T.M., Miri, A., 2015. Primacy of Flexor Locomotor Pattern Revealed by Ancestral Reversion of Motor Neuron Identity. Cell 162, 338–350. doi:10.1016/j.cell.2015.06.036
Marley, R., Baines, R.A., 2011. Whole-Cell Patch Recording from *Drosophila* Larval Neurons. Cold Spring Harb Protoc, 9, 1124-1127.
Matsushima, T., Tegnér, J., Hill, R.H., Grillner, S., 1993. GABAB receptor activation causes a depression of low- and high-voltage-activated Ca2+ currents, postinhibitory rebound, and postspike afterhyperpolarization in lamprey neurons. Journal of Neurophysiology 70, 2606–2619.
Mauss, A.S., Meier, M., Serbe, E., Borst, A., 2014. Optogenetic and pharmacologic dissection of feedforward inhibition in Drosophila motion vision. J Neurosci 34, 2254–2263. doi:10.1523/JNEUROSCI.3938-13.2014
McLean, D.L., Dougherty, K.J., 2015. Peeling back the layers of locomotor control in the spinal cord. Curr Opin Neurobiol 33, 63–70. doi:10.1016/j.conb.2015.03.001
McLean, D.L., Fan, J., Higashijima, S.-I., Hale, M.E., Fetcho, J.R., 2007. A topographic map of recruitment in spinal cord. Nature 446, 71–75. doi:10.1038/nature05588
McLean, D.L., Masino, M.A., Koh, I.Y.Y., Lindquist, W.B., Fetcho, J.R., 2008. Continuous shifts in the active set of spinal interneurons during changes in locomotor speed. Nat Neurosci 11, 1419–1429. doi:10.1038/nn.2225
Miri, A., Azim, E., Jessell, T.M., 2013. Edging toward Entelechy in Motor Control. Neuron 80, 827–834. doi:10.1016/j.neuron.2013.10.049
Nern, A., Pfeiffer, B.D., Rubin, G.M., 2015. Optimized tools for multicolor stochastic labeling reveal diverse stereotyped cell arrangements in the fly visual system. Proceedings of the National Academy of Sciences 112, E2967–76. doi:10.1073/pnas.1506763112

715 Ohyama, T., Schneider-Mizell, C.M., Fetter, R.D., Aleman, J.V., Franconville, R.,
716 Rivera-Alba, M., Mensh, B.D., Branson, K.M., Simpson, J.H., Truman, J.W.,
717 Cardona, A., Zlatic, M., 2015. A multilevel multimodal circuit enhances action
718 selection in Drosophila. Nature 520, 633–639. doi:10.1038/nature14297
719 Okado, N., Homma, S., Ishihara, R., Kohno, K., 1990. Distribution patterns of
720 dendrites in motor neuron pools of lumbosacral spinal cord of the chicken. Anat.
721 Embryol. 182, 113–121.
722 Percival, D.B., Walden, A.T., 1993. Spectral Analysis for Physical Applications.
723 Cambridge University Press.
724 Pfeiffer, B.D., Ngo, T.-T.B., Hibbard, K.L., Murphy, C., Jenett, A., Truman, J.W.,
725 Rubin, G.M., 2010. Refinement of tools for targeted gene expression in
726 Drosophila. Genetics 186, 735–755. doi:10.1534/genetics.110.119917
727 Pratt, C.A., Chanaud, C.M., Loeb, G.E., 1991. Functionally complex muscles of the
728 cat hindlimb. IV. Intramuscular distribution of movement command signals and
729 cutaneous reflexes in broad, bifunctional thigh muscles. Exp Brain Res 85, 281–
730 299.
731 Pulver, S.R., Bayley, T.G., Taylor, A.L., Berni, J., Bate, M., Hedwig, B., 2015.
732 Imaging fictive locomotor patterns in larval Drosophila. Journal of
733 Neurophysiology 114, 2564–2577. doi:10.1152/jn.00731.2015
734 Pulver, S.R., Griffith, L.C., 2010. Spike integration and cellular memory in a
735 rhythmic network from Na+/K+ pump current dynamics. Nat Neurosci 13, 53–59.
736 doi:10.1038/nn.2444
737 Rohrbough, J., Broadie, K., 2002. Electrophysiological analysis of synaptic
738 transmission in central neurons of Drosophila larvae. Journal of Neurophysiology
739 88, 847–860.
740 Romanes, G.J., 1964. The motor pools of the spinal cord. Prog. Brain Res. 11, 93–
741 119.
742 Sato, M., Kojima, T., Michiue, T., Saigo, K., 1999. Bar homeobox genes are
743 latitudinal prepattern genes in the developing Drosophila notum whose expression
744 is regulated by the concerted functions of decapentaplegic and wingless.
745 Development 126, 1457–1466.
746 Schaefer, J.E., Worrell, J.W., Levine, R.B., 2010. Role of intrinsic properties in
747 Drosophila motoneuron recruitment during fictive crawling. Journal of
748 Neurophysiology 104, 1257–1266. doi:10.1152/jn.00298.2010
749 Schindelin, J., Arganda-Carreras, I., Frise, E., Kaynig, V., Longair, M., Pietzsch, T.,
750 Preibisch, S., Rueden, C., Saalfeld, S., Schmid, B., Tinevez, J.-Y., White, D.J.,
751 Hartenstein, V., Eliceiri, K., Tomancak, P., Cardona, A., 2012. Fiji: an open-
752 source platform for biological-image analysis. Nat. Methods 9, 676–682.
753 doi:10.1038/nmeth.2019
754 Stepien, A.E., Tripodi, M., Arber, S., 2010. Monosynaptic rabies virus reveals
755 premotor network organization and synaptic specificity of cholinergic partition
756 cells. Neuron 68, 456–472. doi:10.1016/j.neuron.2010.10.019
757 Sürmeli, G., Akay, T., Ippolito, G.C., Tucker, P.W., Jessell, T.M., 2011. Patterns of
758 spinal sensory-motor connectivity prescribed by a dorsoventral positional
759 template. Cell 147, 653–665. doi:10.1016/j.cell.2011.10.012
760 Sweeney, S.T., Broadie, K., Keane, J., Niemann, H., O'Kane, C.J., 1995. Targeted
761 expression of tetanus toxin light chain in Drosophila specifically eliminates
762 synaptic transmission and causes behavioral defects. Neuron 14, 341–351.
763 Talpalar, A.E., Bouvier, J., Borgius, L., Fortin, G., Pierani, A., Kiehn, O., 2013. Dual-
764 mode operation of neuronal networks involved in left-right alternation. Nature

500, 85–88. doi:10.1038/nature12286
Talpalar, A.E., Endo, T., Löw, P., Borgius, L., Hägglund, M., Dougherty, K.J., Ryge, J., Hnasko, T.S., Kiehn, O., 2011. Identification of minimal neuronal networks involved in flexor-extensor alternation in the mammalian spinal cord. Neuron 71, 1071–1084. doi:10.1016/j.neuron.2011.07.011
Taylor, A.L., Cottrell, G.W., Kleinfeld, D., Kristan, W.B., 2003. Imaging reveals synaptic targets of a swim-terminating neuron in the leech CNS. J Neurosci 23, 11402–11410.
Tripodi, M., Stepien, A.E., Arber, S., 2011. Motor antagonism exposed by spatial segregation and timing of neurogenesis. Nature 479, 61–66. doi:10.1038/nature10538
Wang, W.-C., McLean, D.L., 2014. Selective responses to tonic descending commands by temporal summation in a spinal motor pool. Neuron 83, 708–721. doi:10.1016/j.neuron.2014.06.021
Zwart, M.F., Randlett, O., Evers, J.F., Landgraf, M., 2013. Dendritic growth gated by a steroid hormone receptor underlies increases in activity in the developing Drosophila locomotor system. Proceedings of the National Academy of Sciences 110, E3878–87. doi:10.1073/pnas.1311711110

Figure legends:

Figure 1. Motor neuron intrinsic properties do not contribute to the generation of the intrasegmental motor pattern underlying larval crawling

(A) Longitudinal muscle LO1 (magenta) and transverse muscles LT1-4 (green) in a single segment of the *Drosophila* larva. Left panel shows GFP-labeled muscles of hemisegments A3-A5, schematized in the right panel. **(B)** Contraction pattern of LT2 and LO1 in segment A4 in (A) during a crawling cycle. **(C)** Polar plot of magnitude and phase of coherency of the two waveforms with LO1 as reference. Dashed line indicates α=0.05 for coherence magnitude statistically deviating from 0. Data are represented as mean ±95% confidence interval (CI). Scale bar in (A), 200 µm. **(D, E)** Example motor neurons during patch clamp recording from cell bodies (asterisks) labeled with Alexa Fluor 568 Hydrazide dye, pseudocolored green (D, MN-LT) or magenta (E, MN-LO1). Blue shading is mCD8::GFP expression under the *B-H1* promoter. Scale bar in (D), 5 µm. (**F, G**) Example recordings of MN-LT (F) and MN-LO1 (G), during different levels of current injection. **(H)** Capacitance (C_m), **(I)** membrane resistance (R_m), **(J)** membrane voltage threshold to action potential (V_m threshold), and **(K)** resting membrane potential (V_m rest) of MN-LTs (green) and MN-LO1s (magenta). Boxplots show mean ± quartiles, whiskers minimum to maximum value. $p>0.05$, t-test. The number of action potentials **(L)** and delay to first spike **(M)** as a function of the amplitude of current injection for MN-LTs (green) and MN-LO1s (magenta). There is no statistically significant difference between the slopes of the linear regression lines in (L) ($p>0.05$), and one curve fits best the non-linear fit of (M). n=9 for MN-LTs, n=5 for MN-LO1. Also see Figure S1.

Figure 2. Functionally distinct motor neurons receive divergent input.

(A) Dorsal (left) and posterior (right) views of the reconstructed motor neurons in segment A1 (MN-LTs in green, MN-LO1s in magenta), with efferents (arrowheads) and dendrites (chevrons) indicated. Mesh represents outline of the nervous system, dashed line indicates midline. **(B)** Dorsal (left) and posterior (right) views of the reconstructed interneurons presynaptic to MN-LTs (green, "preLT"), MN-LO1s (magenta, "preLO1") and to both groups of motor neurons (grey, "preCommon"). Scale bars indicate 10µm. **(C)** Force-directed network diagram showing reconstructed motor neurons and all of their presynaptic interneurons. The number of synapses between nodes determines the thickness of edges, which are color-coded according to the identity of the postsynaptic node. In this graph, nodes similar in connectivity will be in close proximity. Motor neurons on the left side of the graph are from the left hemisegment of A1; those on the right are from the right hemisegment. **(D, E)** Overlap in Venn diagrams is proportionate to the number of shared presynaptic partners, with percentage of total input synapses these partners provide indicated. **(F, G)** Pair-wise comparison of relative synaptic contributions of shared presynaptic partners for functionally similar (E) and distinct (F) motor neurons. Also see Figure S2.

Figure 3. Excitatory interneuron eIN-1 innervates transverse motor neurons and is recruited in phase with longitudinal output in the same segment.

Posterior views of ssTEM reconstruction of eIN-1 **(A)** and light microscopy image of R58F03>MCFO (see Experimental Procedures) **(B)**. **(C)** Single optical slice of *SS01970>myrGFP* (expressing in eIN-1) showing pronounced ChAT staining in neurites (arrows). **(D)** Dorsal view of an eIN-1 innervating the contralateral MNs-LTs. **(E)** Electron micrograph showing the apposition of eIN-1 and two MNs-LTs, with presynaptic density indicated (chevrons). **(F)** eIN-1 is presynaptic to MN-DT1 (yellow), which innervates a muscle of similar orientation as the MNs-LTs, a motoneuron innervating an as yet unidentified muscle (cyan), as well as the MNs-LTs (green). Included here are all connections of more than 5 synapses. Muscle diagram indicates identities of known target muscles. **(G)** Stills showing GCaMP6f activity in eIN-1 (blue dashed circles) and MN-aCC (magenta dashed circles) as indicated in schematic, quantified in (H). White arrow and dashed line in (G) indicate approximate front of peristaltic wave. (I) Coherency between eIN-1 and MN-aCC in segment A4 and A3. **(J)** Acute high-intensity optogenetic stimulation (617 nm, 1.1 mW/mm^2) of eIN-1 induces specific contraction of transverse muscles. (K-K') Low-level chronic stimulation of eIN-1 (617 nm, 0.01 mW/mm^2) causes transverse muscles to contract earlier in the locomotor cycle, quantified in (L). Grey lines in (L) indicate individual preparations, black line represents mean. Hotelling paired test, $p<0.05$ for (L) and (X). n=10 stimulations for (J), n=5 animals for GCaMP imaging experiments, n=7 for (K, L). Data are represented as mean ± 95% CI in (I), mean ± SD in (J) and (L). Scale bar indicates 5 µm in (C), 10 µm in (G). See also Figs. S3, S4, and S5.

Figure 4. The intrasegmental motor pattern is sensitive to picrotoxin (PTX).

(A, B) Muscle imaging data showing contraction of muscles LT2 (green) and LO1 (magenta) during a single peristaltic wave before (A) and after (B) bath-application of 10^{-6} M PTX, quantified in **(C, D)**. Control data are the same as in Fig. 1. Scale bar in (B), 200µm. Arrows in (A, B) indicate muscles contracting. **(E)** Coherency between muscles LT2 and LO1 before and after bath-application of PTX in individual animals. **(F)** Phase relationship between muscles LT2 and LO1 before and after bath-application of PTX. Grey lines indicate individual preparations, black line represents mean. $p<0.01$, Hotelling paired test. n=5. Data are represented as mean ± 95% CI in (E), ± SD in (F).

Figure 5. The inhibitory interneuron iIN-1 specifically innervates transverse motor neurons and shows wave-like activity during fictive locomotion.

Posterior view of ssTEM reconstruction **(A)** and light microscopy data **(B)** of iIN-1. **(C)** Immunohistochemical labeling of *R83H09>myrGFP* showing pronounced GABA staining. **(D)** Dorsal view of an iIN-1 innervating contralateral cluster of MNs-LT. **(E)** Electron micrograph showing the apposition of iIN-1 and an MN-LT. **(F)** iIN-1 is presynaptic to other motor neurons innervating muscles of similar orientation as the MNs-LTs. Cyan motor neurons innervate unknown muscles, grey node indicates interneuron. Included in this diagram are all connections of more than 5 synapses. Muscle diagram indicates identity of known target muscles, color-coded according to the left panel. **(G)** Stills showing GCaMP6f activity of iIN-1 and aCC motor neurons as indicated in schematic, quantified in **(H)**. **(I)** Coherency between iIN-1 and aCC motor neurons in segment A5 and A6. Data are represented as mean ±95% CI in (I), n=5. Scale bar represents 5µm in (C), 10µm in (G).

Figure 6. The output of iIN-1 is required to generate the intrasegmental motor pattern.

(A) Contraction of muscles LT2 (green) and LO1 (magenta) in a *+/UAS-Kir2.1* control animal (A) and an *R83H09>Kir2.1* animal (A'), the coherency between which is quantified in **(B). (C)** Phase relation between muscles LT2 and LO1 for various genotypes tested. Pair-wise Watson-Williams test, p=0.003, p=0.004, and p=0.0005 for *R83H09>Kir2.1*, *SS01411>Kir2.1*, and *SS01411>TeTxLC*, respectively ($n \geq 5$). Boxplots show mean ± quartiles, whiskers minimum to maximum value. **(D)** Expression patterns of GAL4-drivers used in this experiment, enlarged in (D'). **(E)** Acute high-intensity optogenetic stimulation (617 nm, 1.1 mW/mm^2) of iIN-1 induces specific relaxation of the transverse muscles. Mean ± SEM of 10 trials. **(F)** Low-level chronic stimulation of iIN-1 (617 nm, 0.1 mW/mm^2) causes transverse muscles to contract later in the locomotor cycle. (F) Mean ± SEM of 10 consecutive contractions of muscles LO1 and LT2 in the same animal pre-stimulation, (F') during stimulation. **(G)** The phase delay between muscle LO1 and LT2 contractions is enhanced in response to low-level chronic stimulation of eIN-1 (617 nm, 0.1 mW/mm^2). Grey lines indicate individual preparations ± SD, black line represents mean. $p<0.05$, Hotelling paired test, n=7. See also Figure S6.

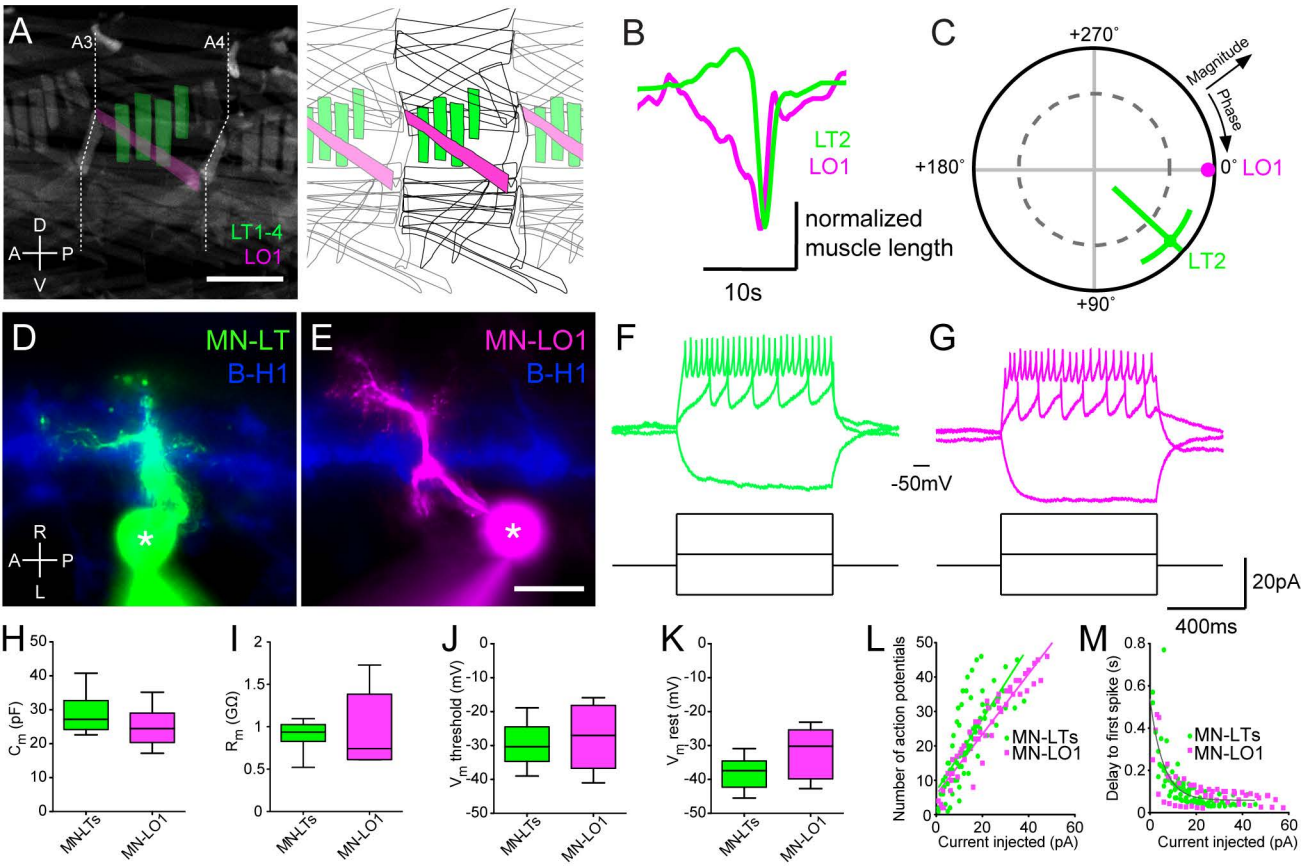
A
A3
A4
D
A
P
V
LT1-4
LO1
B
LT2
LO1
normalized
muscle length
10s
C
+270˚
Magnitude
Phase
+180˚
0˚ LO1
LT2
+90˚
D
MN-LT
B-H1
R
A
P
L
E
MN-LO1
B-H1
F
G
-50mV
20pA
400ms
H
C_m (pF)
MN-LTs
MN-LO1
I
R_m (GΩ)
MN-LTs
MN-LO1
J
V_m threshold (mV)
MN-LTs
MN-LO1
K
V_m rest (mV)
MN-LTs
MN-LO1
L
Number of action potentials
MN-LTs
MN-LO1
Current injected (pA)
M
Delay to first spike (s)
MN-LTs
MN-LO1
Current injected (pA)

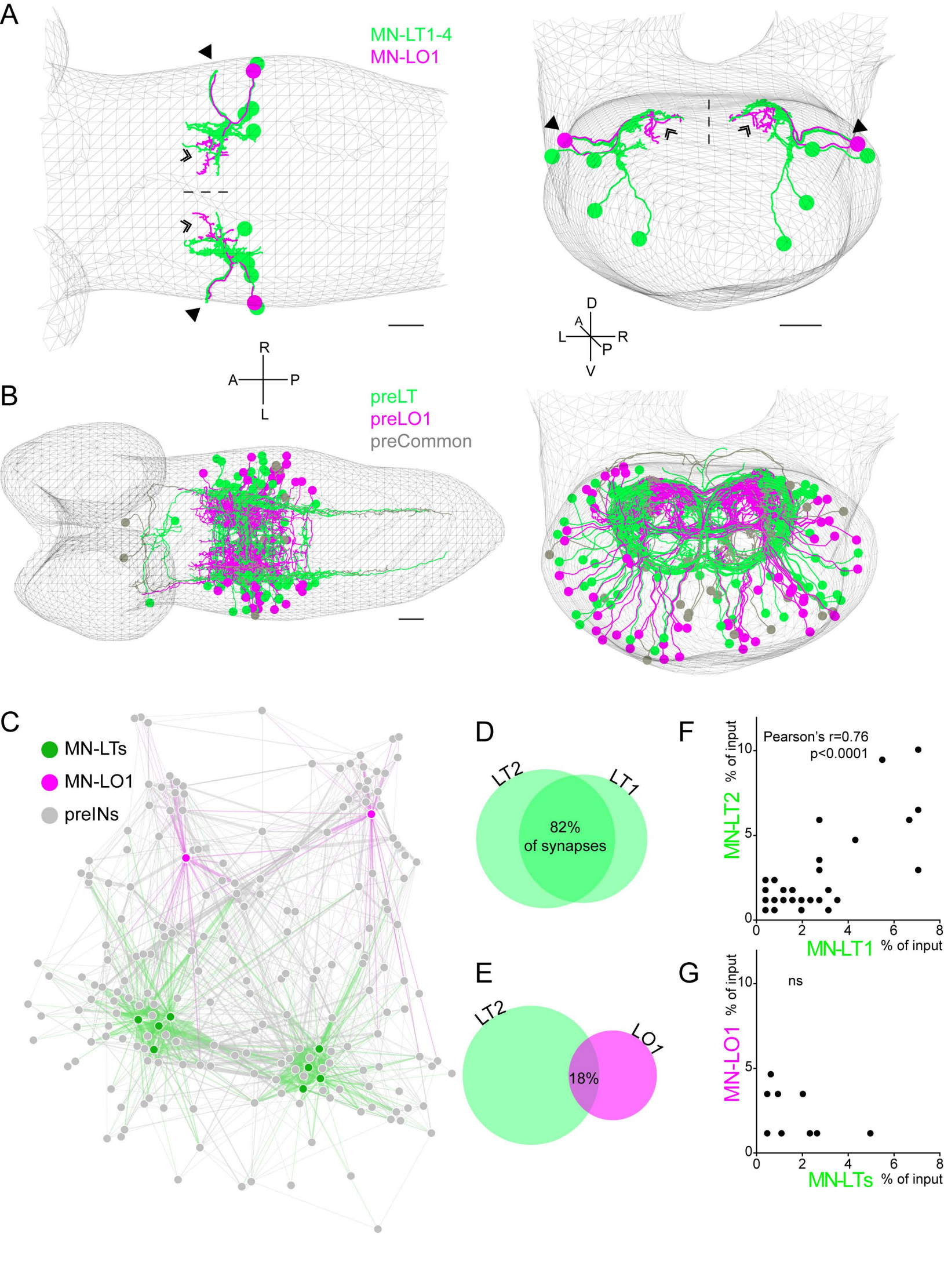
A
MN-LT1-4
MN-LO1
R
A
P
L
D
A
L
R
P
V
B
preLT
preLO1
preCommon
C
MN-LTs
MN-LO1
preINs
D
LT2
LT1
82%
of synapses
E
LT2
LO1
18%
F
Pearson's r=0.76
p<0.0001
MN-LT2 % of input
MN-LT1 % of input
0
2
4
6
8
0
5
10
G
ns
MN-LO1 % of input
MN-LTs % of input
0
2
4
6
8
0
5
10

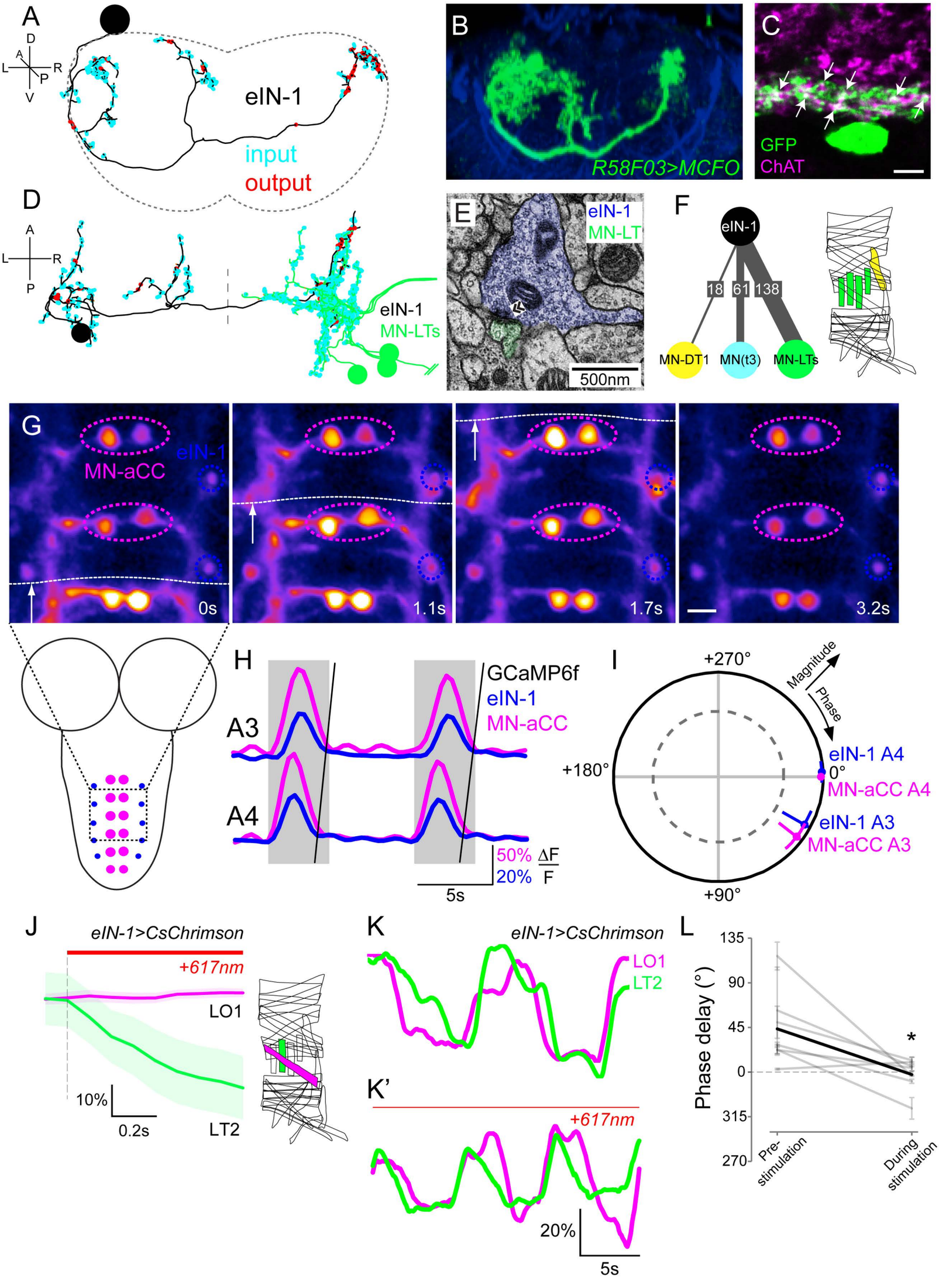
A
D
A
L
R
P
V
eIN-1
input
output
B
R58F03>MCFO
C
GFP
ChAT
D
A
L
R
P
eIN-1
MN-LTs
E
eIN-1
MN-LT
500nm
F
eIN-1
18
61
138
MN-DT1
MN(t3)
MN-LTs
G
MN-aCC
eIN-1
0s
1.1s
1.7s
3.2s
H
GCaMP6f
eIN-1
MN-aCC
A3
A4
50% ΔF
20% F
5s
I
+270°
Magnitude
Phase
+180°
0°
+90°
eIN-1 A4
MN-aCC A4
eIN-1 A3
MN-aCC A3
J
eIN-1>CsChrimson
+617nm
LO1
LT2
10%
0.2s
K
eIN-1>CsChrimson
LO1
LT2
K'
+617nm
20%
5s
L
Phase delay (°)
135
90
45
0
315
270
*
Pre-stimulation
During stimulation

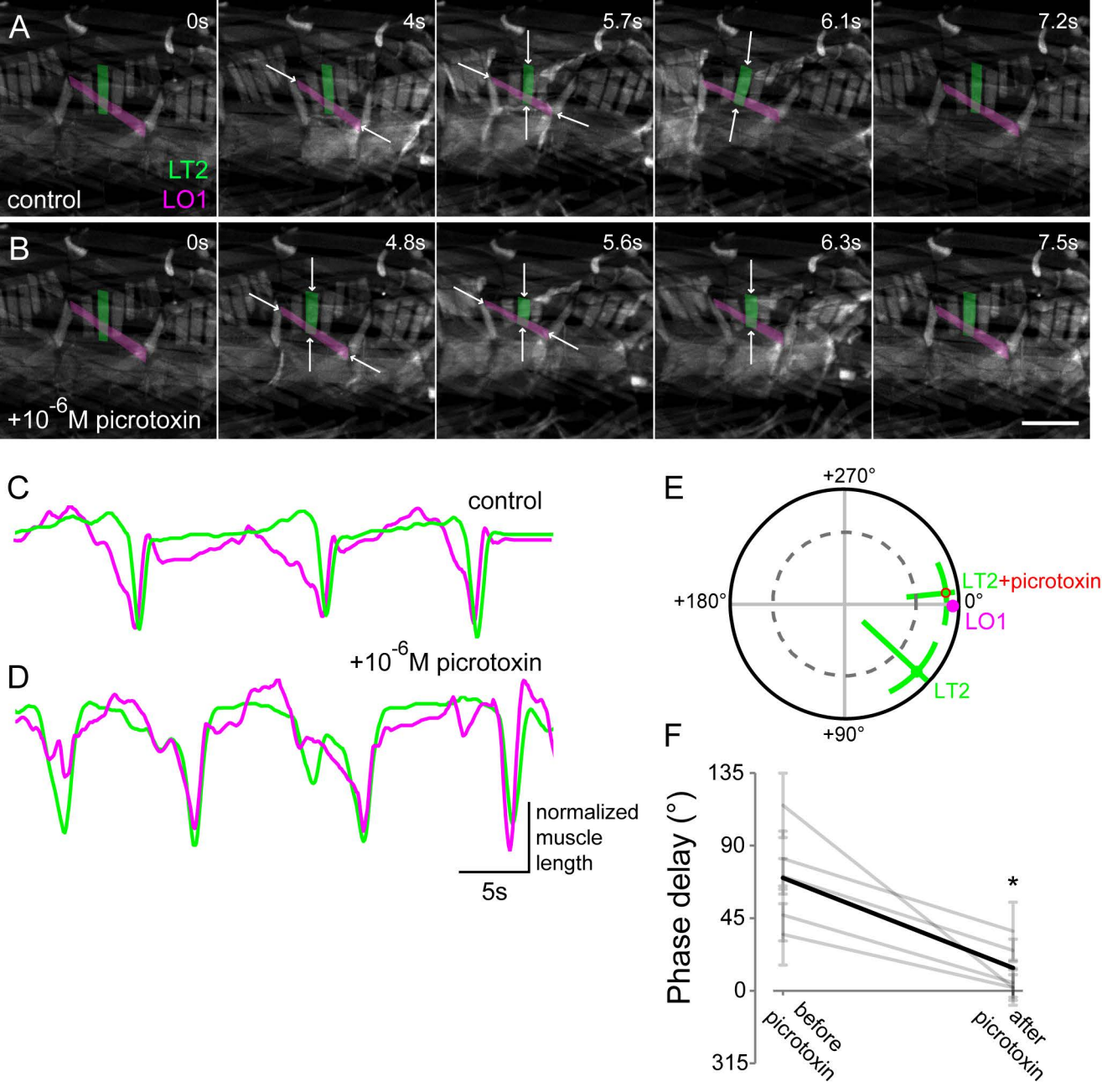
A
0s
4s
5.7s
6.1s
7.2s
LT2
LO1
control
B
0s
4.8s
5.6s
6.3s
7.5s
+10-6M picrotoxin
C
control
D
+10-6M picrotoxin
normalized muscle length
5s
E
+270°
+180°
0°
+90°
LT2+picrotoxin
LO1
LT2
F
Phase delay (°)
135
90
45
0
315
*
before picrotoxin
after picrotoxin

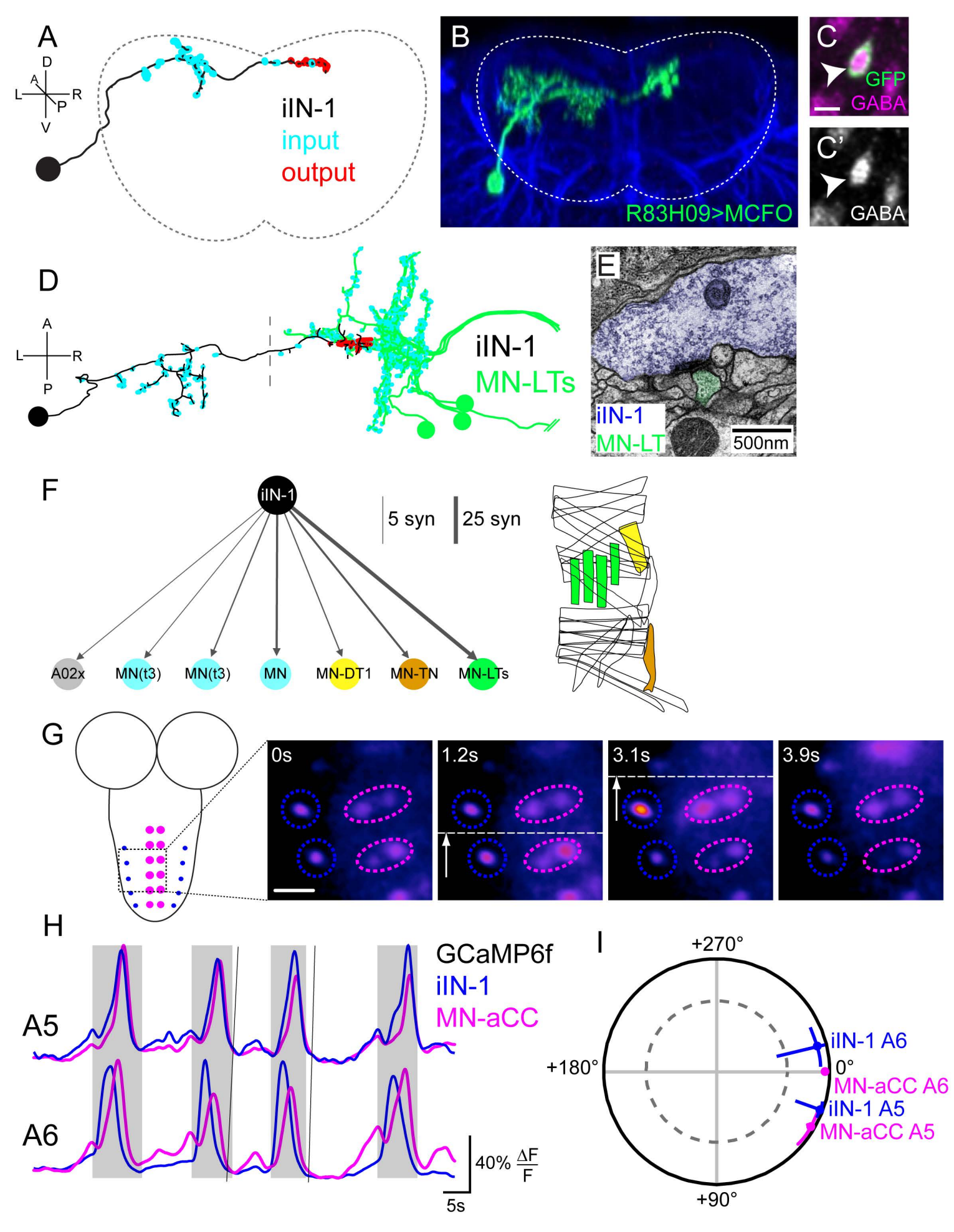
A
D
A
L
R
P
V
iIN-1
input
output
B
R83H09>MCFO
C
GFP
GABA
C'
GABA
D
A
L
R
P
iIN-1
MN-LTs
E
iIN-1
MN-LT
500nm
F
iIN-1
5 syn
25 syn
A02x
MN(t3)
MN(t3)
MN
MN-DT1
MN-TN
MN-LTs
G
0s
1.2s
3.1s
3.9s
H
GCaMP6f
iIN-1
MN-aCC
A5
A6
40% ΔF/F
5s
I
+270°
+180°
0°
+90°
iIN-1 A6
MN-aCC A6
iIN-1 A5
MN-aCC A5

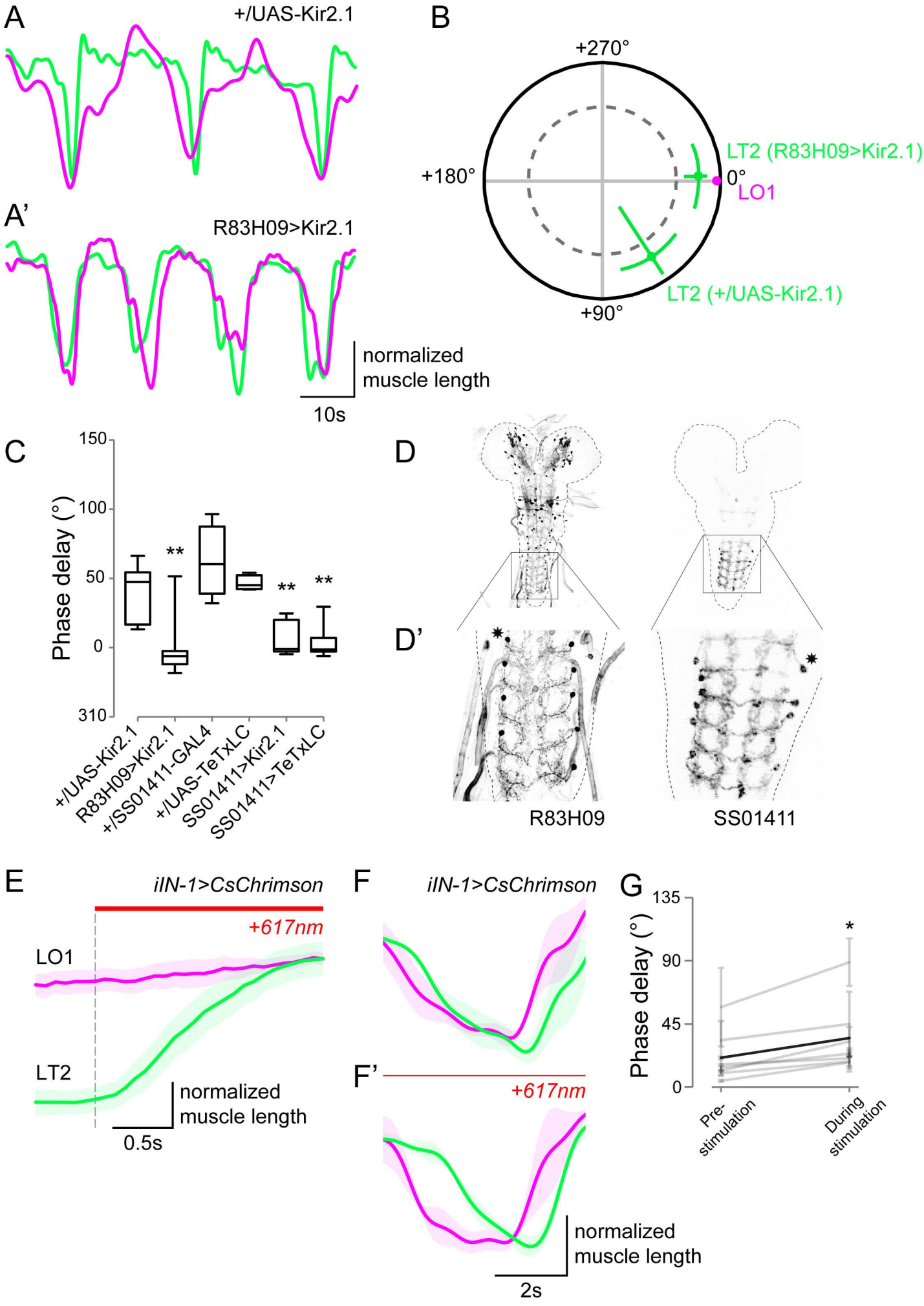
A
+/UAS-Kir2.1
A'
R83H09>Kir2.1
normalized
muscle length
10s
B
+270°
+180°
0°
+90°
LT2 (R83H09>Kir2.1)
LO1
LT2 (+/UAS-Kir2.1)
C
Phase delay (°)
150
100
50
0
310
**
**
**
+/UAS-Kir2.1
R83H09>Kir2.1
+/SS01411-GAL4
+/UAS-TeTxLC
SS01411>Kir2.1
SS01411>TeTxLC
D
D'
R83H09
SS01411
E
iIN-1>CsChrimson
+617nm
LO1
LT2
normalized
muscle length
0.5s
F
iIN-1>CsChrimson
F'
+617nm
normalized
muscle length
2s
G
Phase delay (°)
135
90
45
0
*
Pre-
stimulation
During
stimulation

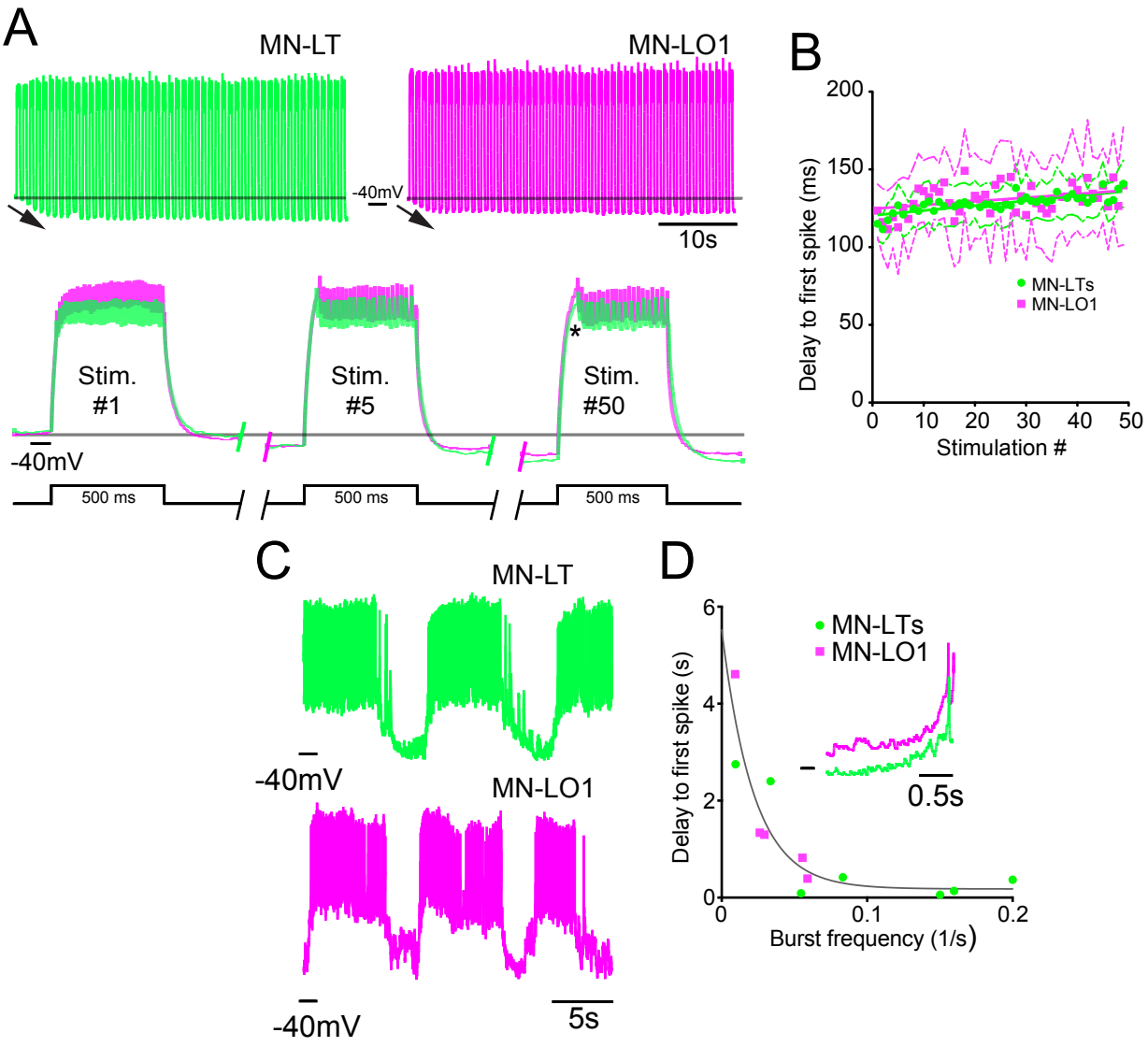

Figure S1, related to Figure 1. Motoneuron intrinsic properties do not contribute to the generation of the intrasegmental motor pattern underlying larval crawling.

(A) Top panels represent example traces of current clamp recordings of an MN-LT and MN-LO1 while repeatedly injecting 20 pA of current for 500 ms per stimulation. Horizontal line indicates resting membrane potential before experiment; arrow emphasizes downward trend after repeated stimulation. Bottom panels show overlaid traces of experiment for stimulation #1, #5 and #50. Asterisk in #50 indicates the change in the delay to first spike. (B) Quantification of delay to first spike as a function of stimulation number for MN-LT and MN-LO1. Plot shows mean delay to first spike (squares) ± SEM (dashed lines). Solid lines indicate linear regression fits. There is no statistically significant difference between either the slopes ($p=0.77$) or intercepts ($p=0.51$) of the two fits. n=5 for MN-LO1, n=9 for MN-LTs. (C) Example traces of current clamp recordings of an MN-LT and MN-LO1 during fictive crawling in two different preparations. Motoneurons fire action potentials as the result of endogenous activity within the motor system. (D) Quantification of delay to first spike, as measured from the start of depolarization to the first action potential, as a function of burst frequency. Solid grey line indicates non-linear fit of the data. One curve fits both data sets best ($p=0.17$). Inset is expanded view of traces in (C) showing similar delay to first spike. n=5 for MN-LO1, n=7 for MN-LTs.

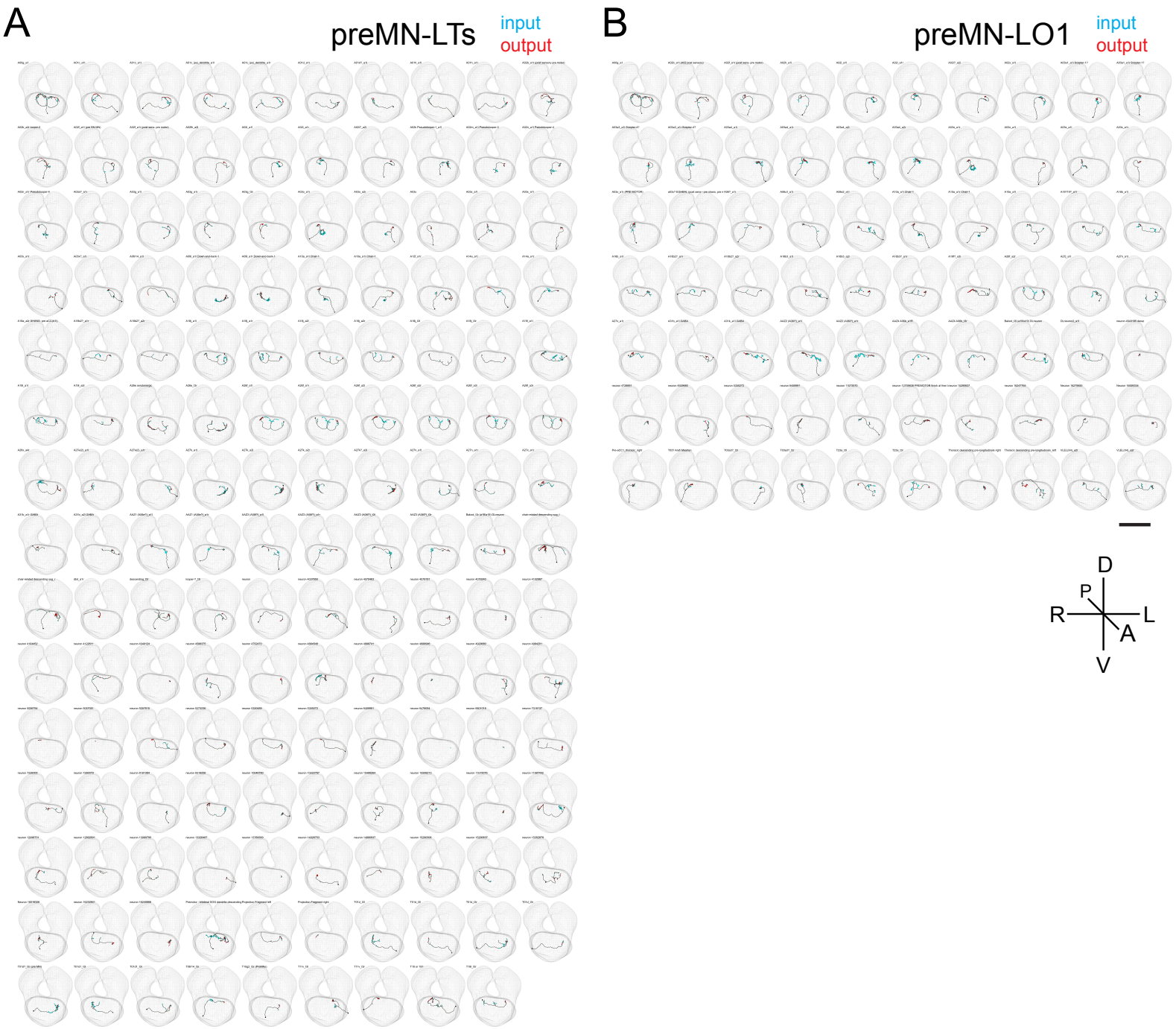

Figure S2, related to Figure 2. Functionally distinct motoneurons receive divergent input.
(A, B) Anterior views of individual reconstructions of all premotor interneurons reconstructed for this study. Scale bar indicates 50 µm.

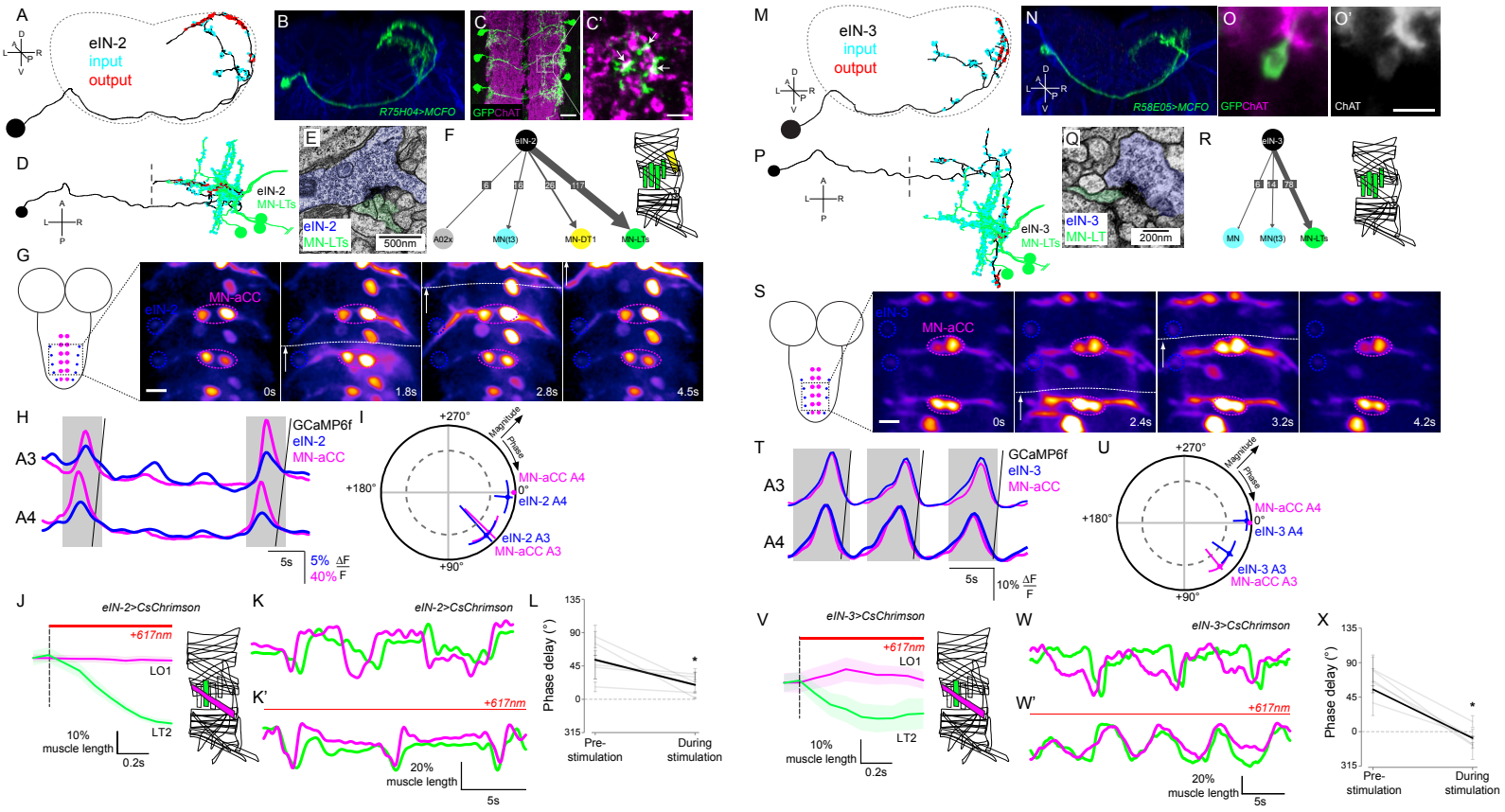

Figure S3, related to Figure 3. eIN-2 and eIN-3 innervate MN-LTs and are recruited during locomotion.
Posterior view of EM reconstruction and light microscopy data of eIN-2 (A,B) and eIN-3 (M,N). (C, O) Immunohistochemical labeling of SS02065>myrGFP (C) and SS01379>GFP (O) showing pronounced ChAT staining. (D, P) Dorsal view of an eIN-2 (D) and eIN-3 (P) innervating contralateral MN-LTs. (E, Q) Electron micrograph showing the apposition of eIN-2 and two LT motoneurons (E) and an eIN-3 with a single MN-LT (Q), with synaptic vesicles and the presynaptic density clearly visible. (F, R) Connectivity diagram of eIN-2 and eIN-3. eIN-2 also innervates the DT1 motoneuron, which innervates a muscle of similar orientation as the MN-LTs. Blue motoneuron innervates unknown muscles (segmental identity in brackets), grey node indicates interneuron. Included in this diagram are all postsynaptic neurons with a connection to eIN-2 and eIN-3 of more than 5 synapses. Muscle diagram indicates identity of known target muscles. (G-I, S-U) eIN-2 and eIN-3 show wave-like activity during fictive crawling. (G, S) Stills showing GCaMP6f activity in eIN-2 and eIN-3 and aCC motoneurons as indicated in schematic, quantified in (H) and (T). (I, U) Coherency between eIN-2 and eIN-3 and aCC motoneurons in segments A3 and A4. (J, V) Acute high-intensity optogenetic stimulation (617 nm, 1.1mW/mm^2) of eIN-2 and eIN-3 induces contraction of the transverse muscles, as measured by muscle-imaging experiments in semi-intact preparations (see Experimental Procedures). LO1 does not contract in response to optogenetic stimulation of eIN-2 or eIN-3. (K, W) Low-level chronic stimulation of eIN-2 and eIN-3 (617 nm, 0.01 mW/mm^2) causes the transverse muscles to contract earlier in the locomotor cycle. (K, W) Quantification of contraction of LO1 and LT2 muscles pre-stimulation, (K', W') during stimulation. (L, X) The phase delay between LO1 and LT2 is reduced in response to low-level chronic stimulation of eIN-2 (L) and eIN-3 (X). Grey lines indicate individual preparations, black line represents mean. Hotelling paired test, $p<0.05$ for (L) and (X). n=10 stimulations for (J) and (V), n=5 animals for all other experiments. Data are represented as mean ± 95% CI in (I) and (U), mean ± SD in (J), (L), (V), and (X). Scale bars in (C), (G), (O'), and (S) indicate 10µm, 1µm in (C').

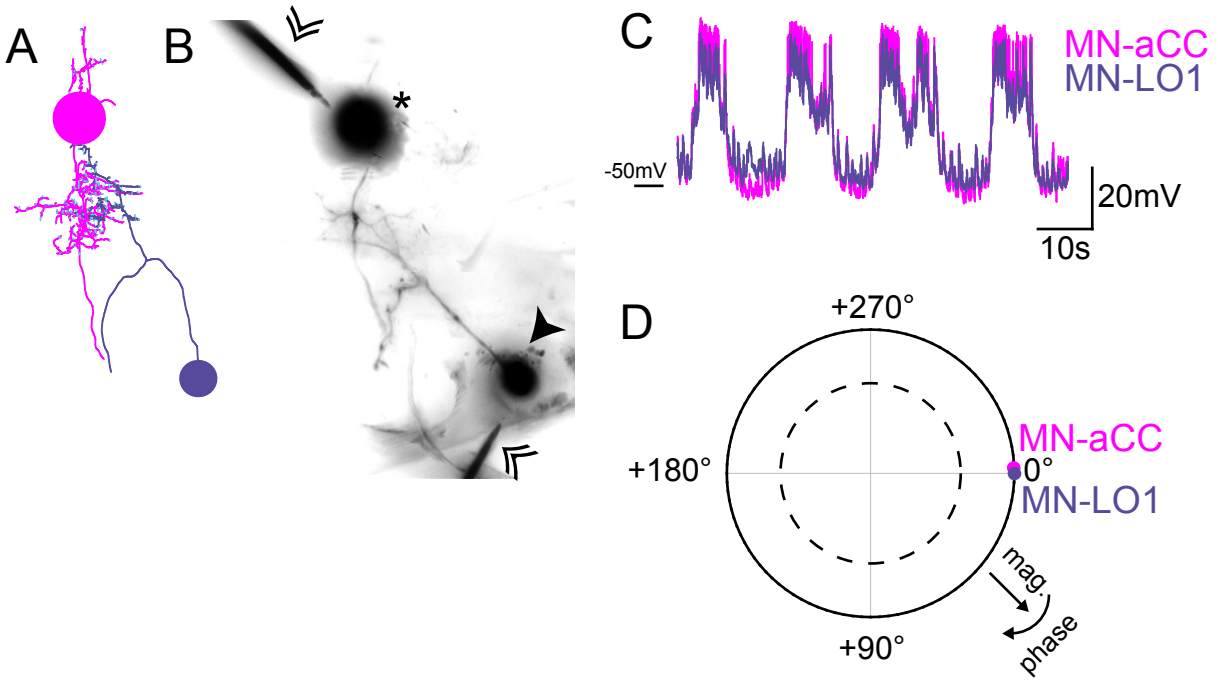

Figure S4, related to Figure 3. MN-LO1 is active in phase with MN-aCC.
(A) Dorsal view of EM reconstruction of MN-aCC (magenta) and MN-LO1 (violet) within the same segment. (B) Example recording of an MN-aCC (asterisk) and an MN-LO1 (arrowhead), showing recording electrodes (chevrons). Cells are visualized by Alexa 568 dye added to the intracellular solution. (C) Traces of simultaneous whole cell recording in current clamp of MN-aCC (magenta) and MN-LO1 (violet), showing membrane voltage fluctuations and action potentials that occur as the result of spontaneous fictive crawling. (D) Coherency between MN-aCC motoneuron and MN-LO1. MN-aCC and MN-LO1 are highly coherent with one another and are very close in phase. n=4.

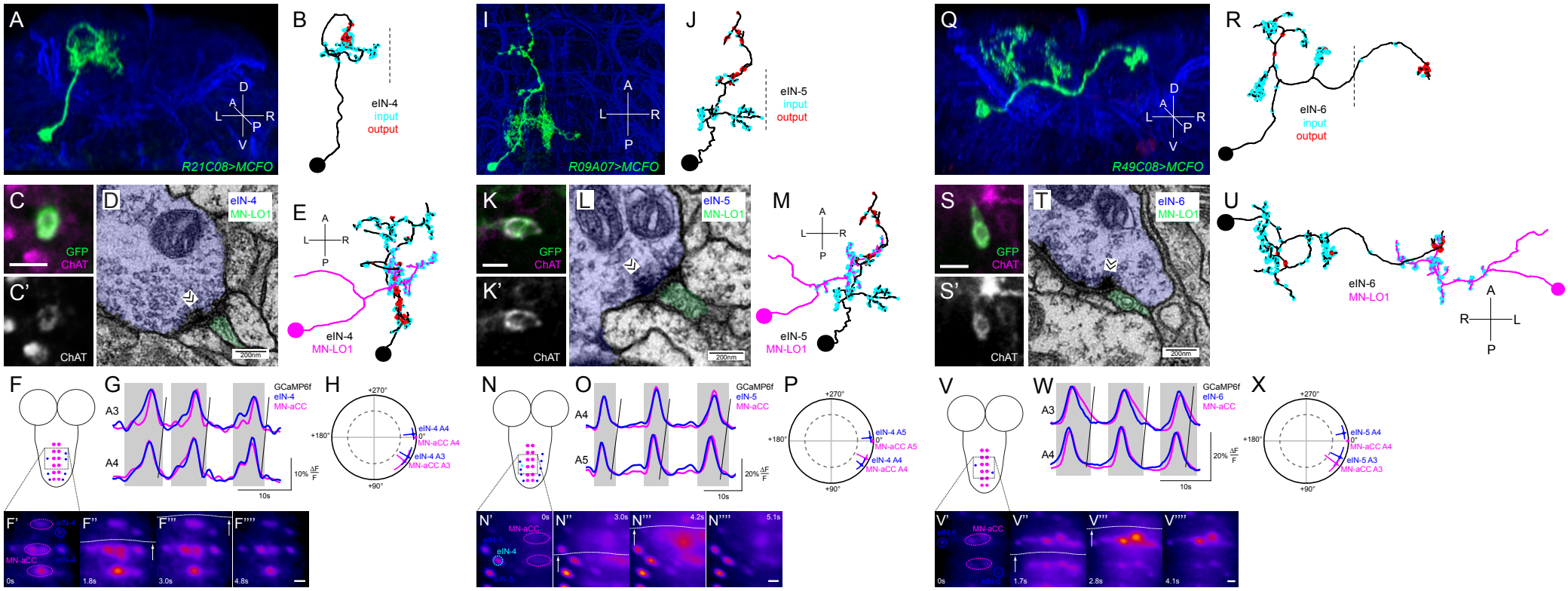

Figure S5, related to Figure 3. eIN-4, eIN-5 and eIN-6 innervate MN-LO1 and are recruited during locomotion.
Posterior (A, R) and dorsal view (J) of EM reconstructions and light microscopy data (B, K, S) of eINs innervating MN-LO1. (C, K, S) Immunohistochemical labeling of SS01956>myrGFP (C), R09A07>myrGFP (K) and SS01404>myrGFP (S) showing pronounced ChAT staining. (D, L, T) Electron micrograph showing the apposition of eINs and MN-LO1, with synaptic vesicles and the presynaptic density clearly visible (chevrons). (E, M, U) Dorsal view of EM reconstructions of eINs innervating MN-LO1, either ipsilaterally (E, M) or contralaterally (U). (F-H, N-P, V-X) eINs show wave-like activity during fictive crawling. (F'-F'''', N'-N'''', V'-V'''') Stills showing GCaMP6f activity in eINs and aCC motoneurons as indicated in schematics (F, N, V), quantified in (G, O, W). (H, P, X) Coherency between eINs and aCC motoneurons in segment A3 and A4 or A4 and A5. Data are represented as mean ± 95% CI in (H), (P), and (X). n=5 for GCaMP imaging experiments, scale bars represent 10µm in (C, F''''), 5µm in (K, N'''', S, and V'''').

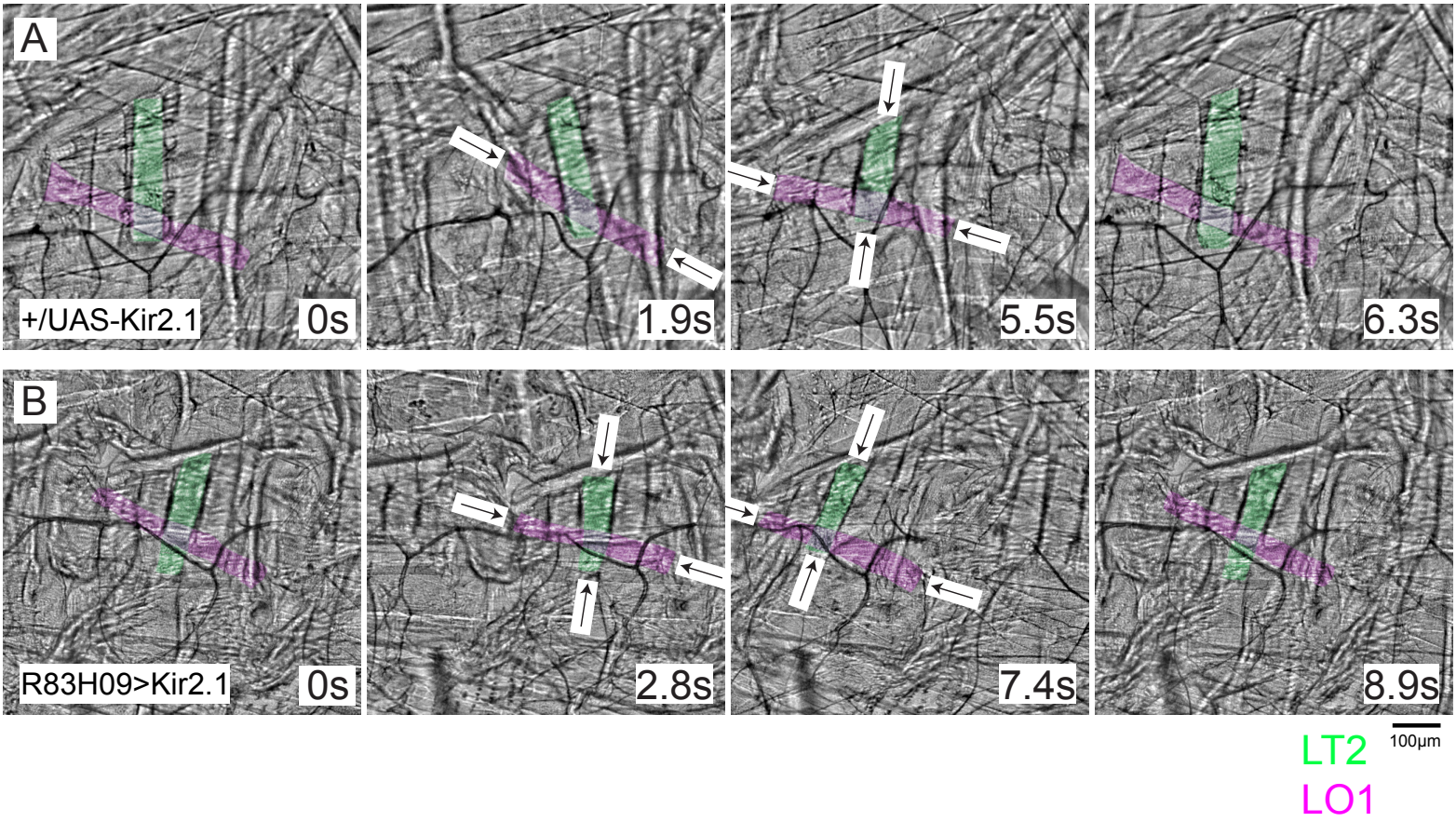

Figure S6, related to Figure 6. Inhibiting iIN-1 leads to a loss of the intrasegmental motor pattern.
(A, B) Stills of imaging experiments to quantify muscle contraction patterns of LT2 (green) and LO1 (magenta) in a +/UAS-Kir2.1 control (A) and R83H09>Kir2.1 (B) preparation. Arrows indicate muscles contracting. See also Figure 6.